Further improvement and evaluation of nudging in the E3SM Atmosphere Model version 1 (EAMv1)

Shixuan Zhang[1], Kai Zhang[1], Hui Wan[1], and Jian Sun[1,2]

[1]Pacific Northwest National Laboratory, Richland, Washington, USA

[2]National Center for Atmospheric Research, Boulder, CO, USA

Correspondence: Shixuan Zhang (Shixuan.Zhang@pnnl.gov) and Kai Zhang (Kai.Zhang@pnnl.gov)

Abstract. A previous study on the use of nudging in EAMv1 had an unresolved issue, namely a simulation nudged to EAMv1's own meteorology showed non-negligible deviations from the free-running baseline simulation over some of the subtropical marine stratocumulus and trade cumulus regions. Here, we demonstrate the deviations can be substantially reduced by ~~two changes in the nudging implementation: first, revising the sequence of calculations in~~ (1) changing where nudging tendency is calculated in the time integration loop of a nudged EAM simulation to improve the consistency with the free-running baseline ~~; second,~~ and (2) increasing the frequency of constraining data ~~from 6-hourly to 3-hourly~~ to better capture strong sub-diurnal variations.

The resulting improvements in ~~climate representativeness motivate an investigation on~~ the climate representativeness provide motivation for an investigation of the potential benefits of using newer reanalysis products with higher data frequency in nudged hindcast simulations that aim at capturing the observed weather events. Simulations using EAMv1's standard horizontal resolution (approximately 1^o) are nudged towards 6-hourly ERA-Interim reanalysis ~~or~~ and 6-hourly, 3-hourly, and hourly ERA5 reanalysis; These simulations are evaluated against the climatology of free-running EAMv1 ~~'s own climatology , global-scale satellite retrievals of outgoing longwave radiation and precipitation,~~ simulations as well as reanalyses, satellite retrievals, and in-situ ~~measurements of air temperature, humidity, and winds~~ measurements from the Atmospheric Radiation Measurement (ARM) user facility. ~~Our overall recommendation is to use the revised sequence of~~ For the 1^o EAMv1 simulations, we recommend using the relocated nudging tendency calculation and 3-hourly ~~data from~~ ERA5 ~~for the nudged simulations~~reanalysis.

~~The anthropogenic aerosol effects in various~~ Simulations aiming at estimating the anthropogenic aerosol effect (F_{aer}) often use nudging to help discern signal from noise. The sensitivity of such estimates to the details of the nudging configuration is investigated in EAMv1~~simulations are evaluated. For~~ , again using the standard 1^o horizontal resolution. It is found that when estimating the global mean ~~effect~~F_{aer}, the source and frequency of constraining data ~~has~~ have a relatively small impact while the selection of nudged variables can change the results substantially. Consistent with ~~conclusions from~~ previous studies, ~~in order to obtain estimates of global mean aerosol effects that are consistent with results~~ we find that the simulated ice cloud formation is sensitive to whether air temperature in EAMv1 is constrained by reanalysis. Nudging temperature in addition to horizontal winds to reanalysis leads to F_{aer} estimates that significantly differ from the free-running baseline~~,~~. When nudged towards the free-running baseline, constraining temperature in addition to horizontal winds in EAMv1 can result in a

more constrained meteorological adjustment to the aerosol perturbation, which also leads to a slightly biased estimate. These results suggest that nudging the horizontal winds but not air temperature is ~~recommended.~~ a better choice for estimating the anthropogenic aerosol effect in EAMv1.

1 Introduction

Nudging (or Newtonian relaxation) is widely used ~~to diagnose model sensitivities in climate models caused by model formulation or tuning~~ for diagnosing sensitivities of climate simulations to modifications in model formulation and parameters (Lohmann and Hoose, 2009; Zhang et al., 2012; Separovic et al., 2012; Lin et al., 2016) ~~, computational methods (Wan et al., 2014) or~~ as well as changes in computational methods (e.g., Wan et al., 2014) and external forcing (Kooperman et al., 2012; Zhang et al., 2014). ~~These studies have shown that nudging can help reduce noise in sensitivity experiments resulting from natural variability,~~ It has been shown that by constraining the large-scale meteorological conditions (e.g. horizontal winds) toward weather reanalysis or a baseline simulation, nudging can help reduce noise caused by natural variability and hence allow for the detection of signals without ~~requiring~~ long simulations or large ensembles (e.g., Kooperman et al., 2012). However, nudging should be used with care. The configuration of the nudged simulations must be carefully evaluated based on the purpose of the ~~study and thoroughly evaluated~~sensitivity experiment. Many studies have shown that the forcing terms introduced by nudging can be sufficiently strong to break the internal balance between ~~dynamics and~~ the resolved dynamics and parameterized physics (e.g. Jeuken et al., 1996) or to cause significant changes in the model's climate (e.g. Zhang et al., 2014), making the results less useful for interpreting the behavior of the original model.

Sun et al. (2019) evaluated two types of nudged simulations conducted with the atmosphere component of the Energy Exascale Earth System Model version 1 (EAMv1, Rasch et al., 2019; Xie et al., 2018) ~~: one type~~ at the standard hoirzontal resolution with approximately 1^o grid spacing. One type of the simulations was constrained by ~~reanalyses products ,~~ reanalysis products and the second type was constrained by ~~the~~ meteorological fields written out from a free-running baseline simulation conducted with the same model (hereafter referred to as the "baseline nudging" method). They showed that simulations using baseline nudging closely resembled the free-running ~~baseline~~ simulation for the key meteorological variables evaluated therein, as evidenced by the high spatial and temporal correlations between the nudged and free-running simulations. On the other hand, systematic decreases in the annual mean shortwave cloud radiative forcing (SWCF) were observed in subtropical and tropical regions when nudging was used, with local annual averages as large as $8\ \mathrm{W\ m^{-2}}$. The discrepancies are inconvenient as they result in inaccuracies in the anthropogenic aerosol effects estimated using ~~baseline-nudging~~baseline nudging.

The study presented here starts with an effort to address these discrepancies. The sequence of calculations related to nudging in EAMv1's time integration ~~cycle~~ loop is reviewed (Sections 2.2 and 3.1) and the time-step-by-time-step temporal evolution of the model state in the subtropics is analyzed (Section 3.2). We demonstrate that the discrepancy issue in 1^o simulations in Sun et al. (2019) can be substantially alleviated by two revisions of the nudging implementation: first, changing the sequence of calculations in a nudged EAM simulation to improve consistency with the free-running baseline; second, increasing the frequency of constraining data from 6-hourly to 3-hourly to better capture strong sub-diurnal variations. The resulting improvements in climate representativeness are presented in Section 3.

Motivated by the improvements, additional simulations and analyses are presented in Section ~~??~~ 4 to explore the potential benefits of using newer reanalysis products with higher data frequency in nudged simulations that aim at capturing the observed weather events. In many previous studies (e.g., Telford et al., 2008; Zhang et al., 2014), the reanalysis products used for generating the nudging data ~~, e. g.~~ were available only 4 times per day. This was the case, for example, for the ERA-Interim reanalysis (Dee et al., 2011) from the European Centre for Medium-Range Weather Forecasts (ECMWF) ~~or the~~ as well as the reanalysis of Kanamitsu et al. (2002) from the National Centers for Environmental Prediction and National Center for Atmospheric Research (NCEP/NCAR)~~Reanalysis (Kanamitsu et al., 2002), were only available 4 times per day~~. In recent years, reanalysis data with ~~high~~ higher temporal frequency are emerging. For example, MERRA-2 (Gelaro et al., 2017) from the ~~NASA GMAO~~ National Aeronautics and Space Administration's Global Modeling and Assimilation Office is available every 3 hours, while the ERA5 reanalysis from ECMWF (Hersbach et al., 2020) ~~provides~~ has hourly data. On the one hand, using high-frequency reanalysis data for nudging may ~~provide a better constraint for the nudged~~ better constrain a simulation. On the other hand, ~~it will increase the computational cost, since the nudging data need to be processed in advance and read in~~ processing more data before and during a simulation ~~. Handling higher frequency nudging data requires more storage and more I/O access~~will consume more resources for data processing and storage. Therefore, it is useful to evaluate the benefit of using high-frequency ~~reanalysis~~ nudging data. Furthermore, since ERA5 is a new reanalysis product that has not been widely used for nudged simulations, it is useful to compare simulations nudged towards ERA5 and ERA-interim, evaluate hindcast skills of these simulations, and provide a recommendation. For ~~this purpose~~those purposes, we present in Section ~~??~~ 4 simulations constrained using 6-hourly ERA-Interim reanalysis ~~or~~ and 6-hourly, 3-hourly, or hourly ERA5 reanalysis. Hindcast skills of the nudged ~~EAM~~ 1^o EAMv1 simulations are evaluated against global-scale satellite retrievals of outgoing longwave radiation and precipitation, as well as in-situ measurements of air temperature, humidity, and horizontal winds from the Atmospheric Radiation Measurement (ARM) user facility. Since one of our primary interests in using nudged simulations is to efficiently estimate the climate impact of anthropogenic aerosols ~~, we also present some analysis on~~ (F_{aer}), we present in Section 5 some analysis of the sensitivity of the ~~estimates~~ estimate to nudging implementation~~in Section 5~~. Our findings and recommendations are summarized in Section 6.

2 Model and simulations

2.1 A brief overview of EAMv1

E3SM is a global Earth system model developed by the U.S. Department of Energy (Golaz et al., 2019). The present study focuses on nudging applications in the E3SM Atmosphere Model version 1 (EAMv1; Rasch et al., 2019; Xie et al., 2018). EAMv1 uses the hydrostatic spectral element (SE) dynamical core on a cubed-sphere mesh (Dennis et al., 2012; Taylor et al., 2010) to solve the equations for large-scale dynamics and tracer transport. The key subgrid-scale physical processes considered in EAMv1 include deep convection (hereafter Deep Cu; Zhang and McFarlane, 1995), turbulence and shallow convection

(Golaz et al., 2002; Larson et al., 2002), cloud microphysics (Morrison and Gettelman, 2008; Gettelman and Morrison, 2015; Wang et al., 2014), aerosol life cycle (Liu et al., 2016; Wang et al., 2020), and radiation (Iacono et al., 2008; Mlawer et al., 1997). EAMv1 is interactively coupled with a land model (Oleson et al., 2013).

Figure 1a shows the sequence of dynamics and physics calculations (i.e., the time integration loop) in EAMv1. More detailed descriptions of the time stepping and coupling of physics and dynamics can be found in ~~? and Wan et al. (2021)~~ Zhang et al. (2018) and Wan et al. (2021, 2022). One important feature relevant to the discussion below is that most of the atmospheric processes are numerically coupled using sequential splitting. This means after a model component (e.g., a parameterization) predicts the rate-of-change (also called tendency) of the model state caused by the atmospheric process it represents, the model state will be updated using the predicted tendency before being handled to the next model component (e.g., another parameterization).

The ~~model used in this study has~~ simulations presented in this paper use a horizontal resolution of approximately 1° (∼110 km). There are 72 layers in the vertical, extending from the Earth's surface to ∼0.1 hPa (∼64 km). The vertical grid spacing is uneven, with the layer ~~height ranging from 20–100 m~~ thickness ranging typically from 20 m to 100 m near the surface and up to 600 m near the model top.

2.2 Nudging in EAMv1

The nudging implementation in EAMv1 was described and evaluated in Sun et al. (2019), so we only provide a brief introduction here. Nudging constrains the model solution toward prescribed atmospheric conditions for a certain variable by adding a relaxation term to the prognostic equation:

$$\left(\frac{\partial X_m}{\partial t}\right)_{\rm ndg} = -\frac{X_m - X_p}{\tau}\,, \qquad (1)$$

where X in Eq. (1) represents a model state variable like horizontal ~~wind~~ winds (U, V), temperature (T), or specific humidity (Q). Subscript m refers to the model-predicted value. Subscript p indicates the prescribed field that is taken or derived from either a global weather reanalysis or a free-running simulation using the same model. τ denotes the relaxation time scale. All three quantities, X_m, X_p, and τ, can affect the sign and strength of the nudging-induced forcing.

Pink boxes in the left panel of Figure 1 illustrate where the nudging-related calculations occur in the default EAMv1. In a nudged simulation, ~~a forcing~~ after the resolved dynamics (see blue box in figure) has been calculated, a nudging tendency term in the form of Eq. (1) is calculated for each nudged ~~prognostic variable ,~~ variable with X_m being the value of X after the dynamical core. ~~These forcing terms are used to update the model state variables after the~~ After the entire physics parameterization suite ~~(before the next call of the dynamical core). When~~ has been calculated, the sum of the parameterization-induced tendencies and the nudging tendencies are passed to the physics-dynamics coupling interface.

It is worth noting that, when an EAM simulation is considered to be a baseline simulation, the dynamical and thermodynamical variables (e.g., U, V, T, Q, and the surface pressure PS) that are archived – and ~~used subsequently~~ subsequently used in a nudged simulation as the prescribed atmospheric state – are the values saved before the radiation calculation (cf. pink dashed box in Fig. 1a). In other words, in the default EAMv1, the X_p in the right-hand side of Eq. (1) is archived before radiation while the X_m in that same equation corresponds to the model state after the dynamical core. As is discussed in Section 3.1, the fact that X_p and X_m correspond to different locations in the time integration loop plays an important role in causing the issue in Sun et al. (2019) that motivated this study.

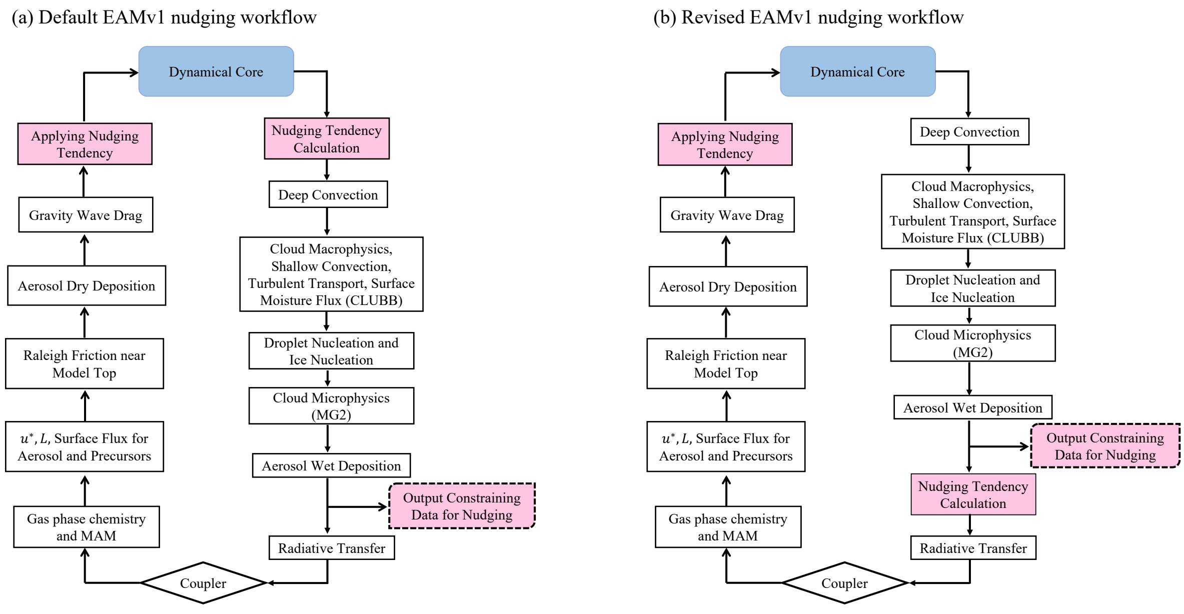

Figure 1. Flowcharts showing the sequence of dynamics and physics calculations within one time step in an EAMv1 simulation. Pink boxes indicate where the nudging-related calculations occur. Panel (a) is adapted from Fig. S1 in Sun et al. (2019) and corresponds to the default EAMv1 code. Panel (b) is the revised sequence of ~~calculation~~ calculations evaluated in this study. The key difference is that in panel (b), the calculation of nudging tendency using Eq. (1) occurs at the same location where the prescribed meteorological state is written out in the baseline simulation, i.e., before the radiation parameterization. Panel (b) is described in detail in Section 3.1.

2.3 Simulations

The EAMv1 simulations presented in this paper are summarized in Table 1. All the simulations involved active atmosphere and land but used prescribed sea surface temperature (SST) and sea ice extension, following the protocol from the Atmospheric Model Intercomparison Project (Gates et al., 1999). The SST and ~~sea ice~~ sea-ice extension used in this study are weekly data from the National Oceanic and Atmospheric Administration (NOAA) Optimum Interpolation (OI) analysis (Reynolds et al., 2002). Other external forcings, including volcanic aerosols, solar variability, concentrations of greenhouse gases, and anthropogenic emissions of aerosols and their precursors, were prescribed following the World Climate Research Programme (WCRP) Coupled Model Intercomparison ~~Project-Phase~~ Project Phase 6 (CMIP6; Eyring et al., 2016; Hoesly et al., 2018; Feng et al., 2020). ~~Emissions of aerosols and their precursor gases of the year 2010 are used to represent the present-day (PD) condition.~~

All simulations were performed from 1 October 2009 to 31 December 2010. The first 3 months were discarded as model spin-up, and the remaining 1 year of model output was used for analysis. The choice of simulation year was based on convenience, as hourly ERA5 data of 2010 were readily available to us. Sun et al. (2019) have shown that the annual mean cloud radiative forcing and its shortwave and longwave components derived from 1-year nudged simulations ~~were~~ are representative of the corresponding longer-term (e.g., 5-year) statistics (see, e.g., Fig. 19 therein).

~~The first group of simulations~~ To estimate the anthropogenic aerosol effect F_{aer}, pairs of simulations were conducted. Each pair had identical experimental setup except that the emissions of aerosols and their precursor gases were set to the values of the year 2010 to represent the present-day (PD) condition in one simulation and the values of the year 1850 to represent the pre-industrial (PI) condition in the second simulation. The greenhouse gas concentrations, SST, and sea ice extent are unchanged (i.e., fixed at their year-2010 values). The main differences between PI and PD aerosol emissions include anthropogenic sulfur, black carbon, organic carbon, primary organic carbon, and SOA precursors (applied as yields) emissions. Biomass burning emissions are also slightly changed from the PD condition to PI . Dust, sea salt, and marine organic aerosol emissions are calculated online using the surface wind speed and surface properties predicted in each simulation.

Three groups of simulations are presented in this paper~~is an ensemble of five~~ . The first group consists of five pairs of 15-month simulations. The first ~~ensemble member is a~~ pair is two free-running baseline ~~simulation~~ simulations referred to as CLIM PD and CLIM PI in the remainder of the paper~~, from which~~ . From the CLIM PD simulation, the before-radiation values of U, V, T, Q, and PS were archived at 1-hour, 3-hour, and 6-hour frequencies to constrain some of the subsequent simulations. The other four ~~ensemble members~~ pairs in group one were nudged to 6-hourly temperature output from ~~CLIM~~ the CLIM PD simulation but using long relaxation time scales of 10 days, 10.1 days, 10.2 days, 10.3 days, respectively. These relaxation time scales correspond to values of $1/\tau$ on the order of 10^{-6}, which resulted in physically insignificant constraints on the simulations. Therefore, the four ~~ensemble members~~ pairs of nudged simulations can effectively be considered to be free-running although with perturbations introduced to the 3D temperature field that can be used to quantify natural variability in the evolution of the atmospheric state. A similar experimentation strategy has been used by Liu et al. (2018) to generate hindcast ensembles to investigate the radiative forcing of fire-emitted aerosols.

The second group of simulations was ~~constrained by~~ nudged to the meteorology archived from ~~CLIM with nudging applied at all time steps and all vertical levels,~~ the CLIM PD simulation in group 1, regardless of whether the PD or PI emissions were used in the nudged simulations. Nudging was applied at every time step and vertical level using a 6 h relaxation time scale. The ~~two simulations~~ simulations labeled DNDG_UV6 and DNDG_UVT6 used the sequence of ~~calculation~~ calculations shown in Fig. 1a (i.e., the default EAMv1) while RNDG_UV6 and RNDG_UVT6 used the revised sequence shown in Fig. 1b and explained in Section 3.1. The impact of the revised sequence ~~of calculation~~ is evaluated in Section 3.1. The difference ~~in simulation setup between each pair of experiments labeled~~ between experiments labeled with "_UV" and "_UVT" is whether only the horizontal winds were nudged ("_UV") or both winds and temperature were nudged ("_UVT"). The ending number 6 in the experiment names indicates the use of 6-hourly output from CLIM. ~~Two additional pairs of~~ Additional simulations were conducted, also using the revised sequence ~~,~~ of calculations but constrained by 3-hourly or 1-hourly output from ~~CLIM. These two pairs~~ the CLIM PD simulation (RNDG_UV3 and RNDG_UVT3~~,~~ ; RNDG_UV1 and RNDG_UVT1). These simulations are compared with RNDG_UV6 and RNDG_UVT6 in Section 3.2 to evaluate the impact of the frequency of the constraining data .

The third group of simulations was nudged toward two reanalysis products, ERA-Interim (Dee et al., 2011) and ERA5 (Hersbach et al., 2020), to assess whether using a newer product (ERA5) and its higher data frequency, instead of the older ERA-Interim at 6-hour intervals, can provide nudged hindcast simulations that agree better with the observational data. The reanalysis products were spatially remapped to the cubed-sphere grid and 72 model layers used by EAMv1, following the method used in the Community Earth System Model Version 2 (CESM2; https://ncar.github.io/CAM/doc/build/html/users_guide/physics-modifications-via-the-namelist.html#nudging). Topographical differences between EAMv1 and the reanalysis model were taken into account during the vertical interpolation. This group of simulations are compared to global or quasi-global observational data of surface precipitation rate and the top of atmosphere outgoing longwave radiation from satellite retrievals (Section 4.2) as well as in-situ measurements from the Atmospheric Radiation Measurement (ARM) program (Section 4.3).

For selected model configurations (cf. Table 1), we also performed simulations using the pre-industrial (PI, year 1850) aerosol and precursor gas emissions while keeping the greenhouse gas concentrations, SST, and sea ice extent unchanged from the PD simulations. These PI simulations are used to assess the impact of nudging strategy on the estimates of the direct and indirect radiative effects of the anthropogenic aerosols (Section 5).

3 Improving climate representativeness of simulations nudged to CLIM

This section focuses on analyzing the PD simulations listed in group 2 of Table 1. The CLIM PD simulation in group 1 is used as the baseline simulation and referred to as CLIM for brevity.

Before this work, the EAMv1 simulations nudged to 6-hourly output from CLIM were known to show non-negligible differences from CLIM. For example, Fig. 15b in Sun et al. (2019) showed the weakening of 1-year mean SWCF on the order of 2–8 W m^{-2} in large areas of the subtropical marine and coastal regions when horizontal winds and temperature were both nudged. The differences exceeded 8 W m^{-2} in some regions over the southeast Pacific Ocean and South America. Figure 15a in that same paper showed that constraining only the horizontal winds (i.e., no temperature nudging) would remove the discrepancies in most of the subtropical regions, although one would find 4–8 W m^{-2} of strengthening of the annual mean SWCF close to the coast of Peru. The corresponding discrepancies seen in the total cloud forcing (CF) and cloud cover are shown in panels (b) and (d) of Fig. 2 and Fig. A1 in this paper. The CF in this paper is defined as the sum of short-wave and long-wave radiative forcings. When winds and temperature are both nudged, we see a substantial number of grid cells in the subtropical Pacific and Atlantic oceans where the relative differences on the order of 10% to 20% are seen in total CF when compared to the annual mean total CF in the baseline simulation CLIM (Fig. A2d). Discrepancies of such magnitudes are counterintuitive since the constraining data were generated from the same model driven by the same external forcing. On the other hand, since nudging introduces forcing terms in the form of Eq. (1) to the model's governing equations, any differences between X_m and X_p will lead to deviations from a free-running simulation. Below, we show that such deviations can be

Table 1. List of simulations described in Section 2.3. Nudging was applied at each physics time step. A 6-h relaxation time scale was used for group 2 and 3 in the nudged simulations . in groups 2 and 3. For the "CLIMpx" CLIMp1–CLIMp4 simulations, very long relaxation time scales (about 10 days) were applied to generate ensemble members in addition to CLIM. Simulations using The present-day (PD, year 2010) external forcing were carried was used to carry out simulations with all of the listed configurations. Pre-industrial The pre-industrial (PI, year 1850) emissions of aerosols and precursors were used to carry out additional simulations for a subset of the configurations (see the right-most column).

Group number	Simulation short name	Flowchart	Nudged variables	Constraining data and frequency	Nudging relaxation time scale	Aerosol and precursor gas emissions
1	CLIM	Fig. 1a	None	N/A	N/A	PD and PI
1	CLIMp1	Fig. 1a	T	CLIM PD (6 hr)	10.1 days	PD and PI
1	CLIMp2	Fig. 1a	T	CLIM PD (6 hr)	10.2 days	PD and PI
1	CLIMp3	Fig. 1a	T	CLIM PD (6 hr)	10.3 days	PD and PI
1	CLIMp4	Fig. 1a	T	CLIM PD (6 hr)	10.4 days	PD and PI
2	DNDG_UV6	Fig. 1a	U, V.	CLIM PD (6 hr)	6 hr	PD
2	DNDG_UVT6	Fig. 1a	U, V, T	CLIM PD (6 hr)	6 hr	PD and PI
2	RNDG_UV6	Fig. 1b	U, V	CLIM PD (6 hr)	6 hr	PD and PI
2	RNDG_UVT6	Fig. 1b	U, V, T	CLIM PD (6 hr)	6 hr	PD and PI
2	RNDG_UV3	Fig. 1b	U, V	CLIM PD (3 hr)	6 hr	PD and PI
2	RNDG_UVT3	Fig. 1b	U, V,T	CLIM PD (3 hr)	6 hr	PD and PI
2	RNDG_UV1	Fig. 1b	U, V	CLIM PD (1 hr)	6 hr	PD
2	RNDG_UVT1	Fig. 1b	U, V, T	CLIM PD (1 hr)	6 hr	PD
3	DNDG_ERAI_UV6	Fig. 1a	U, V	ERA-Interim (6 hr)	6 hr	PD
3	DNDG_ERAI_UVT6	Fig. 1a	U, V, T	ERA-Interim (6 hr)	6 hr	PD
3	RNDG_ERAI_UV6	Fig. 1b	U, V	ERA-Interim (6 hr)	6 hr	PD
3	RNDG_ERAI_UVT6	Fig. 1b	U, V, T	ERA-Interim (6 hr)	6 hr	PD
3	RNDG_ERA5_UV6	Fig. 1b	U, V	ERA5 (6 hr)	6 hr	PD and PI
3	RNDG_ERA5_UV3	Fig. 1b	U, V	ERA5 (3 hr)	3 hr	PD and PI
3	RNDG_ERA5_UVT6	Fig. 1b	U, V, T	ERA5 (6 hr)	6 hr	PD and PI
3	RNDG_ERA5_UVT3	Fig. 1b	U, V, T	ERA5 (3 hr)	3 hr	PD and PI
3	RNDG_ERA5_UVT1	Fig. 1b	U, V, T	ERA5 (1 hr)	6 hr	PD

significantly reduced by revising the sequence of calculations in nudged simulations and thereby achieving better consistency with the free-running baseline (Section 3.1), as well as by increasing the data frequency of the constraining meteorology to better capture higher-frequency variations in time (Section 3.2).

3.1 Calculation of nudging tendency

As mentioned in Section 2.2, in EAMv1's nudging implementation before this study, the baseline simulation's atmospheric state was archived before the radiation parameterization while the nudging-induced forcing (i.e., Eq. (1)) was calculated after the dynamical core. Since EAMv1 uses sequential splitting to couple most of the atmospheric processes (cf. Section 2.1), if we

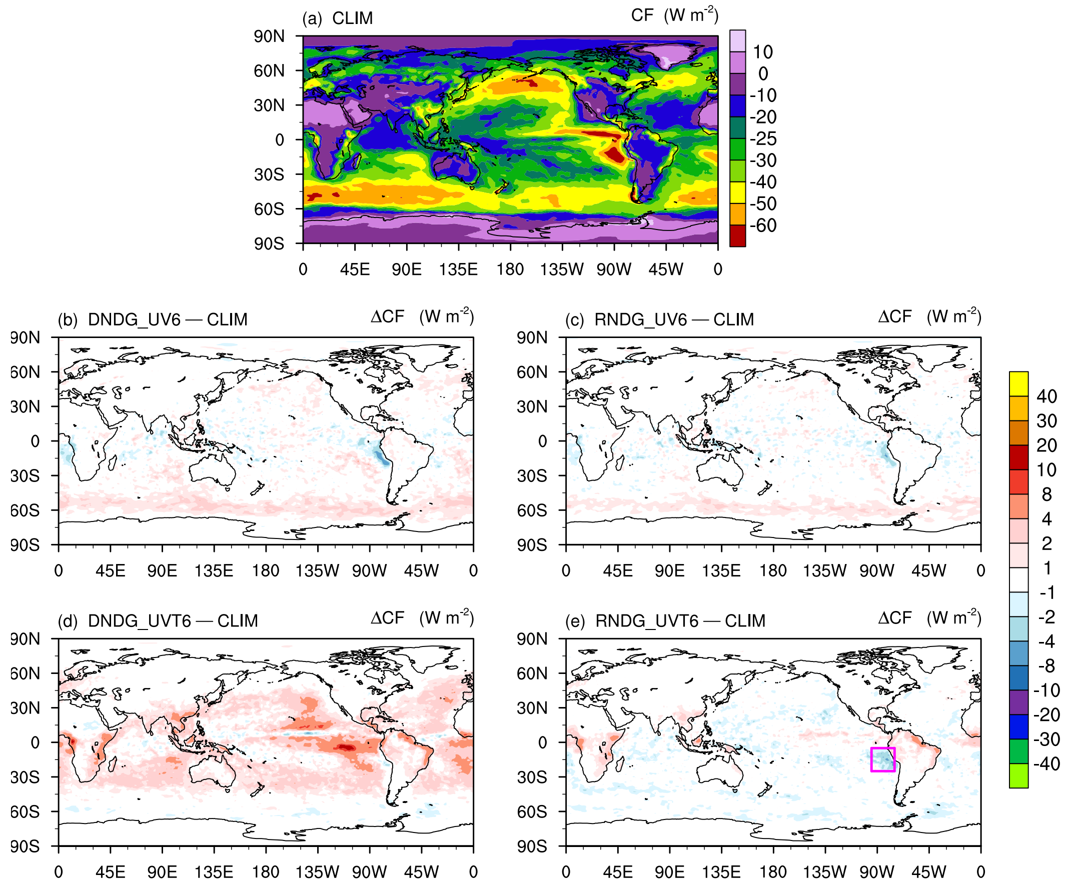

Figure 2. Global annual mean total cloud radiative forcing (CF, unit: W m^{-2}) in the free-running simulation (CLIM, panel a) and the differences between nudged simulations and CLIM (panels b-e). All simulations in this figure used the PD aerosol and precursor emissions. Descriptions of the simulation setups can be found in Section 2.3 and Table 1. The magenta box over the Peruvian stratocumulus region in panel (e) is further analyzed in Fig. 3.

use a subscript "DYN" to label the atmospheric state after the dynamical core and a subscript "ARC" to label the atmospheric state being archived, then the the old nudging implementation was, effectively,

$$\left(\frac{\partial X_m}{\partial t}\right)_{\mathrm{ndg}} = -\frac{X_{\mathrm{m,DYN}} - X_{\mathrm{p,ARC}}}{\tau} \tag{2}$$

$$= \left(-\frac{X_{\mathrm{m,ARC}} - X_{\mathrm{p,ARC}}}{\tau}\right) + \left(\frac{X_{\mathrm{m,ARC}} - X_{\mathrm{m,DYN}}}{\tau}\right) \tag{3}$$

In our understanding, the first term on the right-hand side of Eq. (3) is the intended nudging tendency while the second term is inadvertent. Furthermore, the second term can be understood as the total tendency caused by deep convection, turbulence, and stratiform cloud parameterizations scaled by a factor of $\Delta t/\tau$ where Δt is the physics time step. Since these moist processes are known to strongly affect the atmospheric state, especially temperature and humidity, it is not surprising that nudged simulations using Eq. (2) deviate from their free-running baseline.

When the calculation of the nudging tendency is moved before the radiation parameterization so that X_p from the baseline simulation and X_m in the nudged simulation come from the same location of the time integration cycle (see schematic in Fig. 1b), we ~~will~~ have, as intended,

$$\left(\frac{\partial X_m}{\partial t}\right)_{\rm ndg} = -\frac{X_{\rm m,ARC} - X_{\rm p,ARC}}{\tau}. \tag{4}$$

Sensitivity experiments confirm that using Eq. (4) instead of Eq. (2) ~~signficantly~~ significantly reduces discrepancies between the UVT-nudged and free-running simulations, as can be seen by comparing Fig. 2e with 2d. The annual mean total CF differences are reduced to within 1 W m^{-2} for the majority of the grid cells and within 2 W m^{-2} in the subtropics and tropics, with only a small number of grid cells showing differences between 2–5 W m^{-2}. The discrepancies between UV-nudged and free-running simulations are also reduced, although not as significantly (Fig. 2c versus 2b). The remaining discrepancies are investigated in the next subsection.

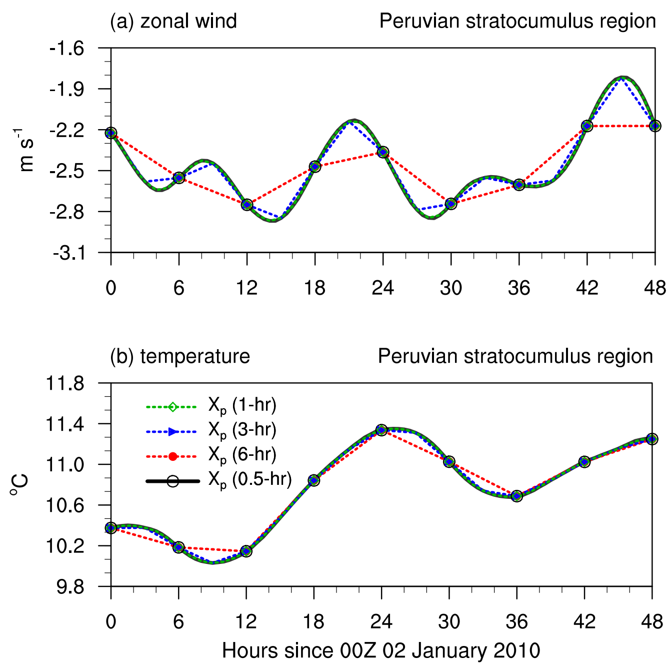

Figure 3. Time evaluation of (a) zonal wind (unit: m s^{-1}) and (b) temperature (unit: ^{o}C) at the model level closest to 700 hPa during a 48-h period starting from 00Z 02 January 2010. The values shown are horizontal averages ~~of~~ over the magenta box in Fig. ~~4~~2e. The black thick lines are time-step-by-time-step output from CLIM. The red, blue, and green lines are time-step-by-time-step values of X_p in Eq. (1) that were obtained by linear temporal interpolation using 6-hr, 3-hr and 1-hr output of CLIM.

3.2 Frequency of constraining data

Nudged simulations in the literature (e.g., Kooperman et al., 2012; Subramanian and Zhang, 2014; Ma et al., 2014, 2015; Lin et al., 2016; Fast et al., 2016), including our own work (e.g., Zhang et al., 2014; Sun et al., 2019), often used 6-hourly constraining data. The historical reason was that reanalysis data used to be available only 4 times per day. Such a frequency, on the other hand, can be insufficient for capturing fast variations because of the problem of aliasing.

Figure 3 shows the evolution of lower-troposphere (700 hPa) zonal wind and temperature averaged over the Peruvian stratocumulus region marked by the ~~red~~ magenta box in Fig. 2e, for a 2-day period starting from 00Z 02 in January 2010. In Fig. 3, the black solid lines are time-step-by-time-step output from CLIM where $\Delta t = 30$ min. The dashed lines are the linearly interpolated time series used in the calculation of nudging tendencies; green, blue, and red correspond to cases in which the constraining data was provided at 1 h, 3 h, and 6 h frequencies, respectively. The EAMv1-simulated wind field in the Peruvian stratocumulus region shows prominent 12 h cycles. Linear interpolation of 6-hourly data misses all the local maxima and minima (red line in Fig. 3a) while the interpolation from 3-hourly data provides substantial improvements (blue line in Fig. 3a). The temperature time series in Fig. 3b also shows 12 h variations although the amplitude is much smaller compared to the diurnal cycle.

Considering the multiscale nature of the atmospheric motions, one can speculate there are modes of variability that need higher than 3-hourly sampling frequency to avoid aliasing. The sensitivity experiments conducted using 6 h, 3 h, and 1 h constraining data (cf. group 2 of Table 1 and Fig. 4), however, suggest that nudged simulations using 3-hourly data can provide annual mean cloud forcing estimates that agree with CLIM within 1 W m^{-2} for most grid cells~~.~~, at least for the 1° simulations considered here. In the future, before nudged simulations are conducted at substantially higher resolutions (e.g., 0.25° or convection-permitting), it will be useful to find out whether the better-resolved fine-scale motions will require higher frequencies of constraining data.

3.3 Climate representativeness beyond cloud radiative forcing

The investigations discussed in Sections 3.1 and 3.2 focused on cloud radiative forcing. In Fig. 5, we further evaluate the climate representativeness of the nudged simulations by assessing the annual averages of twenty 2D fields that are often examined during model development and tuning. ~~For each nudged simulation~~ These fields are labeled along the x-axis in panel Fig. 5d and explained in Appendix A2. For each of the nudged PD simulations listed in group 2 of Table 1 and each of the twenty fields, we calculated two error metrics with respect to ~~CLIM~~the CLIM PD simulation: one measuring the difference in the global annual mean (Fig. 5a-b) and one measuring the root-mean-square difference in the ~~annually averaged~~ annually-averaged global geographical pattern (Fig. 5c-d~~, cf. Appendix A2~~).

Consistent with the cloud forcing results shown in ~~Figures~~Figs. 2 and 4, the revised sequence of ~~calculation~~ calculations and 3 h data frequency have larger impacts on the UVT-nudged simulations than on UV-nudged simulations. Nevertheless, we see a systematic reduction of global mean and pattern errors across all twenty quantities evaluated in Fig. 5 ~~.~~ (i.e., yellow bars are substantially shorter than orange bars; green bars are significantly shorter than yellow bars). In simulations RNDG_UVT3 and

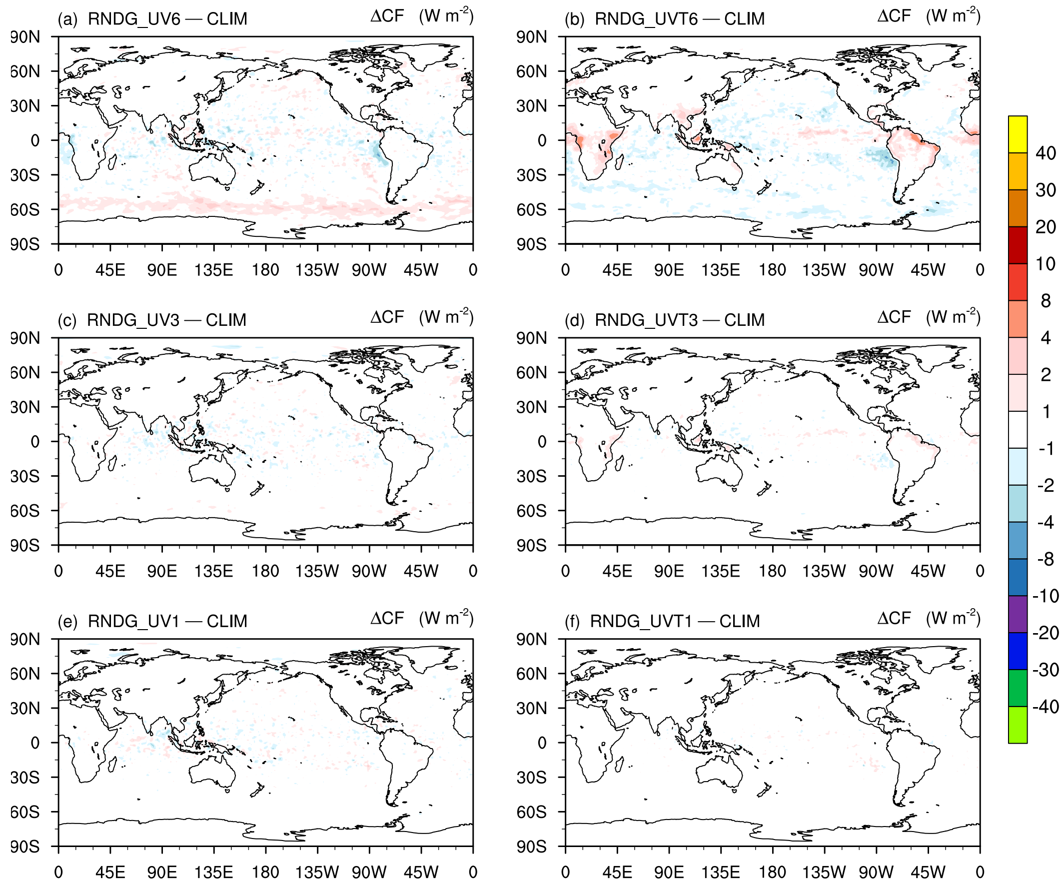

Figure 4. Differences in annual mean total cloud forcing (ΔCF, unit: W m^{-2}) between nudged simulations and CLIM, all using PD (year 2010) forcing conditions. Simulations shown in the left column used only wind nudging while simulations shown in the right column used wind and temperature nudging. From the first row to the bottom row, the frequency of constraining data used in the nudged simulation is 6-hourly, 3-hourly, and hourly, respectively. The simulation setups are described in Section 2.3 and Table 1.

RNDG_UV3, the errors in global averages are reduced to less than 1% ~~.~~ (green bars in Fig. 5a-b). The errors in geographical patterns are reduced to 2% or less for the UVT-nudged simulation and 3% or less for the UV-nudged simulation (~~the lower error~~ green bars in Fig. 5c-d). Comparing panels c and d in Fig. 5, we see lower errors associated with UVT-nudging~~is likely~~ ; this is possibly an indication of better consistency between winds and temperature ~~)~~when both are nudged. Further increase of data frequency to 1 h only leads to limited improvements in the simulated geographical patterns. ~~In addition, we~~ We consistently see the fact that increasing data frequency from 6-hourly to 3-hourly leads to a better agreement of global averages with the free-running simulation, but a further increase to hourly data no longer ~~lead~~ leads to substantial differences~~(cf. Table S2)~~. This can be seen not only in Fig. 5a-b but also in the additional cloud- and precipitation-related quantities shown in Table S1.

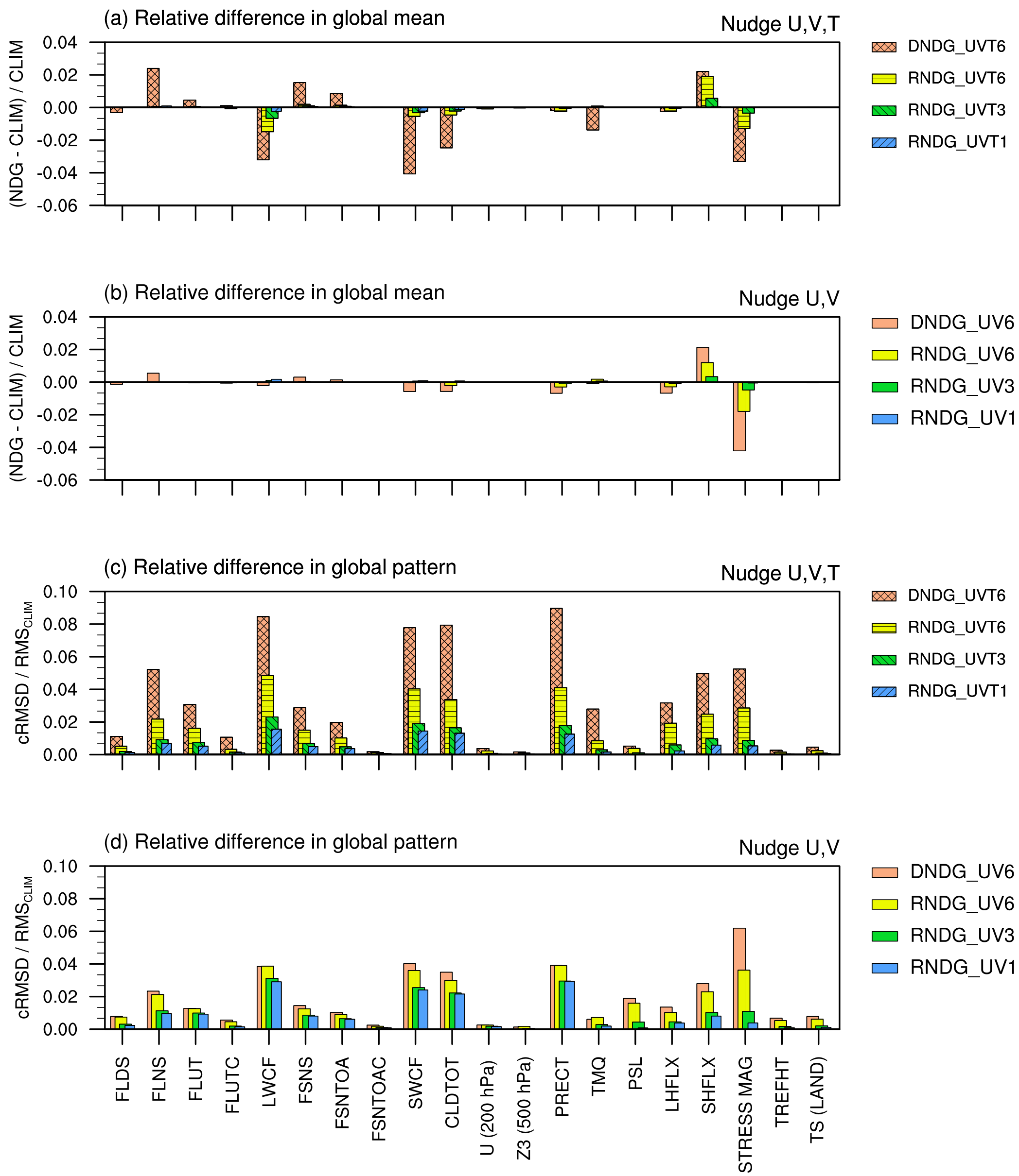

Figure 5. Comparison of annual averages in nudged simulations and CLIM, all using PD (year 2010) forcing conditions. The physical quantities labeled along the x-axis are explained in Table A2. Panels (a) and (b) show relative differences in the simulated global averages. Panels (c) and (d) show relative differences in the simulated geographical distributions. The hatched bars shown in panels (a) and (c) correspond to simulations using wind and temperature nudging; the bars without hatching shown in panels (b) and (d) correspond to simulations using wind-only nudging. Different colors in the same panel indicate different nudging ~~configuration~~ configurations (sequence of ~~calculation~~ calculations and frequency of constraining data). All differences were calculated against CLIM. Further details can be found in Section 3.3 and Appendix A2.

Therefore, for future applications that use 1° simulations nudged to the model's own meteorology, we recommend using the revised sequence of calculation calculations depicted in Fig. 1b and 3-hourly constraining data. UV-nudging and UVT-nudging can give similar results, with the former providing slightly better internal consistencyFuture investigations are needed to find out whether nudged simulations at higher spatial resolutions will require more frequent constraining data.

4 Evaluation of simulations nudged to reanalyses

As mentioned in the introduction, a common application of nudging is to force the simulated large-scale meteorological conditions to follow the trajectory of the observed evolution so as to facilitate process-level model evaluation or composite analyses focused on specific types of weather events. In this case, nudged simulations are typically performed using gridded reanalysis products from an operational weather prediction center as the constraining data. The findings from the previous section, especially the conclusion that higher frequency of the constraining data might help better capture important modes of variability, motivated us to evaluate the potential benefits of using more recent reanalysis products such as ERA5 (Hersbach et al., 2020) and MERRA2 (Gelaro et al., 2017). Since ERA5 has the highest data frequency (i.e., hourly), and ERA5 is also known to show better agreement with observations when compared with its predecessor ERA-Interim (Hersbach et al., 2020), we focus on ERA5-constrained simulations in this section and use the sensitivity experiments listed in group 3 of Table 1 to answer the following questions:

- What is the impact of nudging on the simulated mean climate? (Section 4.1)
- Do ERA5-nudged hindcast simulations agree better with observations than the ERA-Interim-nudged simulations? (Section 4.2)
- How frequently should the nudging data be provided to obtain sufficiently good hindcast skill? (Section 4.3)

The discussion in this section focuses on simulations performed under PD forcing conditions.

4.1 Global and regional mean climate

Since the long-term climate simulated by the free-running EAMv1 is known to have non-negligible biases with respect to observational data (Rasch et al., 2019; Xie et al., 2018), nudging towards reanalysis is expected to result in significant changes in the statistical features of the simulated climate. When U and V are nudged to 6-hourly meteorology from ERA-Interim, the annual mean total CF can deviate from CLIM by more than -20 W m $^{-2}$ in the Californian, Peruvian, and Namibian stratocumulus regions . (Fig. 6a). When T is also nudged, we see deviations on the order of -10 W m $^{-2}$ to -20 W m $^{-2}$ over the storm tracks and 10 W m $^{-2}$ to 40 W m $^{-2}$ over the trade cumulus regions (Figure 6, first row). Noticeable changes in the global mean CF are also evidenced in Fig. 6b). In terms of global averages, nudging only U and V to 6-hourly ERA-Interim data gives a total CF very close to the value in CLIM; the shortwave and longwave components deviate from the corresponding values in CLIM by about 0.3 W m $^{-2}$ (cf. simulation RNDG_ERAI_UV6 in Table S1). If T is nudged in addition to U and

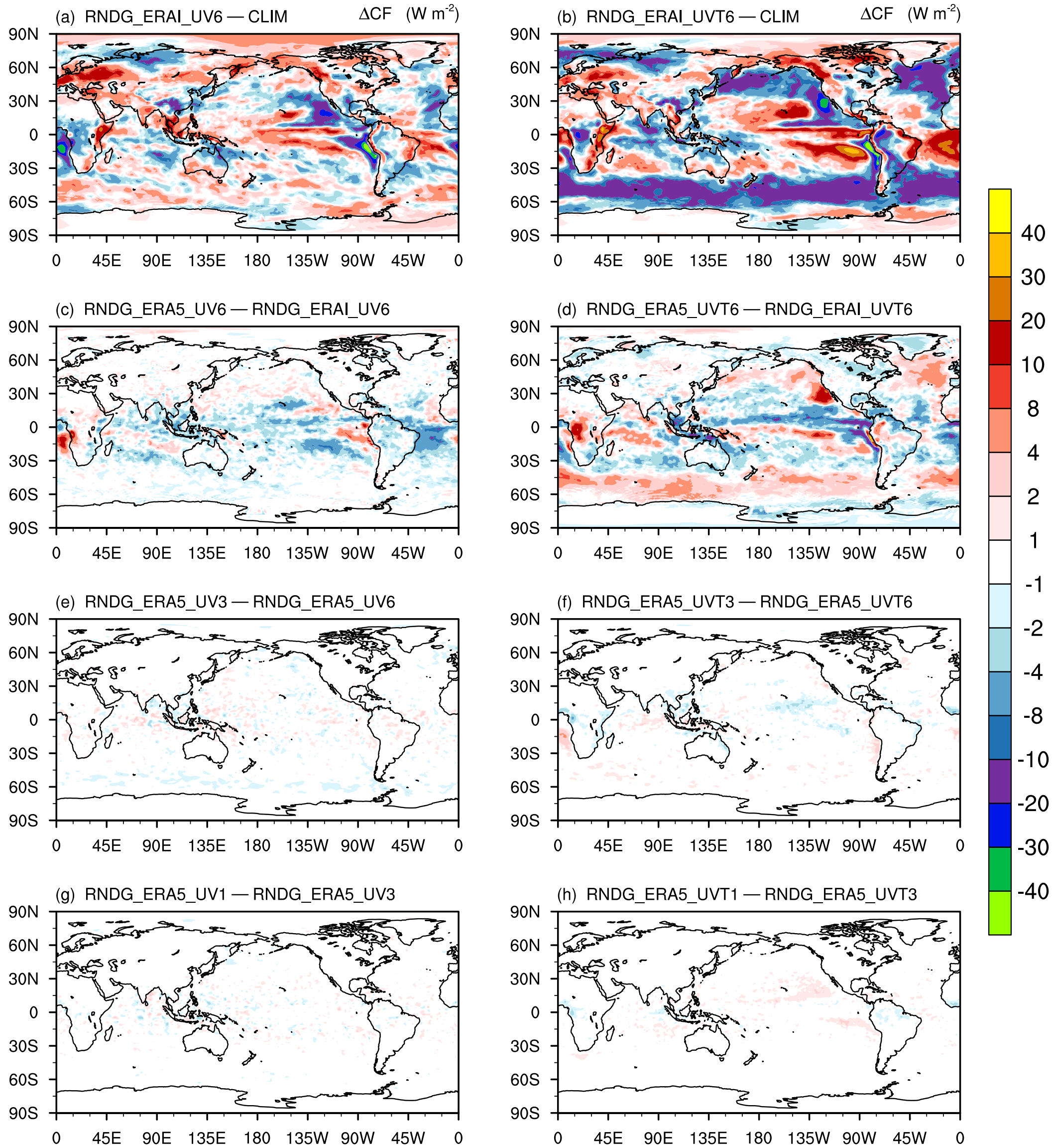

Figure 6. Annual mean differences in the total cloud forcing (ΔCF, unit: W m^{-2}) ~~.~~ in PD simulations of the year 2010. The top row shows the differences between simulations nudged to ERA-Interim and ~~without nudging~~ the free-running baseline (CLIM). The second row shows differences between simulations nudged to ERA5 and ERA-Interim, both using 6-hourly constraining data temporally interpolated to every model time step. The third ~~(fourth)~~ row shows the differences between simulations that interpolate 3-hourly ~~(1-hourly)~~ versus 6-hourly reanalysis data to constrain the model simulated meteorology. The last row is like the third row, but showing differences between two simulations nudged to hourly versus 3-hourly reanalysis data interpolated to model time steps. The left and right columns correspond to wind-only nudging and wind-and-temperature nudging, respectively. Details of the simulation setup can be found in Section 2.3 and Table 1.

V, the global mean total CF deviates from the ~~ERA-nudged simulations with UVT nudging, the deviations from CLIM are on the order of -1 to -2~~value in CLIM by about -1.7 W m $^{-2}$, attributable mainly to the longwave component (cf. ~~-~~simulation RNDG_ERAI_UVT6 in Table S2). These results are consistent with ~~Sun et al. (2019)~~ the conclusion from Sun et al. (2019) that ERA-nudged runs differ substantially from CLIM.

The second row of ~~Figure~~Fig. 6 shows the impact of using ERA5 instead of ERA-Interim while keeping a 6-hourly data frequency. The resulting changes are substantially smaller than the differences between ERA-nudged simulations and CLIM, although we still see some CF differences in the subtropics and tropics as large as 10 W m $^{-2}$ to 20 W m $^{-2}$. The relatively small impact of replacing ERA-Interim ~~by~~ with ERA5 is expected, as the differences between ERA5 and ERA-Interim are substantially smaller than the differences between either reanalysis and the free-running EAMv1 simulations. (As an example, the annual mean zonal mean pressure-latitude ~~cross-section~~ cross-sections of air temperature differences are shown in Fig. A3). Increasing the data frequency from 6-hourly to 3-hourly can lead to local changes of 1 to 4 W m $^{-2}$ in CF. These magnitudes are similar to what we have seen in Fig. 4a-d for the simulations nudged to CLIM. Further increasing the data frequency to hourly only introduces negligible changes, again similar to what we have seen in simulations nudged to CLIM (Fig. 4e-f).

A large number of model output variables have been examined in addition to CF, where we consistently see the differences between ERA-Interim-nudged and ERA5 nudged simulations being substantially smaller than the differences between nudged runs and CLIM, although the magnitudes are non-negligible in some regions. We also consistently see the fact that increasing data frequency from 6-hourly to 3-hourly can lead to discernible changes locally while a further increase to hourly data no longer ~~lead~~ leads to substantial differences. The impacts ~~on~~ of data frequency on the simulated global averages are generally very small (cf. Table S2).

4.2 Global and regional weather events

To evaluate the simulation of large-scale weather events, we follow the procedure used for ~~Figure~~Fig. 5 in Sun et al. (2019) and examine the anomaly correlation between nudged simulations and the observations. Here, an anomaly is defined as the deviation of a simulated or observed quantity from the corresponding (simulated or observed) monthly average at the same geographical location. We first examined the anomaly correlation between the nudged simulations and the corresponding reanalysis (ERA-Interim or ERA5) for temperature, specific humidity, as well as horizontal and vertical winds at various pressure levels. The results were found to be very similar to those presented in ~~Figure~~Fig. 5 in Sun et al. (2019). ERA-Interim and ERA5 nudged simulations show similar correlations to the corresponding reanalyses (~~c. f.Figure~~cf. Fig. S1).

Since the discussion in this section focuses on comparing the hindcast skill of the ERA-Interim-nudged and ERA5-nudged simulations, we present in Figs. 7 and 8 an evaluation against global and regional-scale satellite retrievals of outgoing longwave radiation (OLR) and surface precipitation rate. Panel (a) in each figure shows the annual average of spatial correlations in different latitude bands; panel (b) in each figure shows the spatially averaged temporal correlations of the anomalies. In Fig. 7, the two upper rows in each panel compare ~~simulations~~ ERA-Interim-nudged and ERA5-nudged simulations that used wind-only nudging~~and~~ , while the lower rows compare simulations that also used temperature nudging. Figure 8 compares ERA5-nudged simulations that used different data frequencies. The EAM-simulated OLR is compared with National Oceanic and Atmospheric

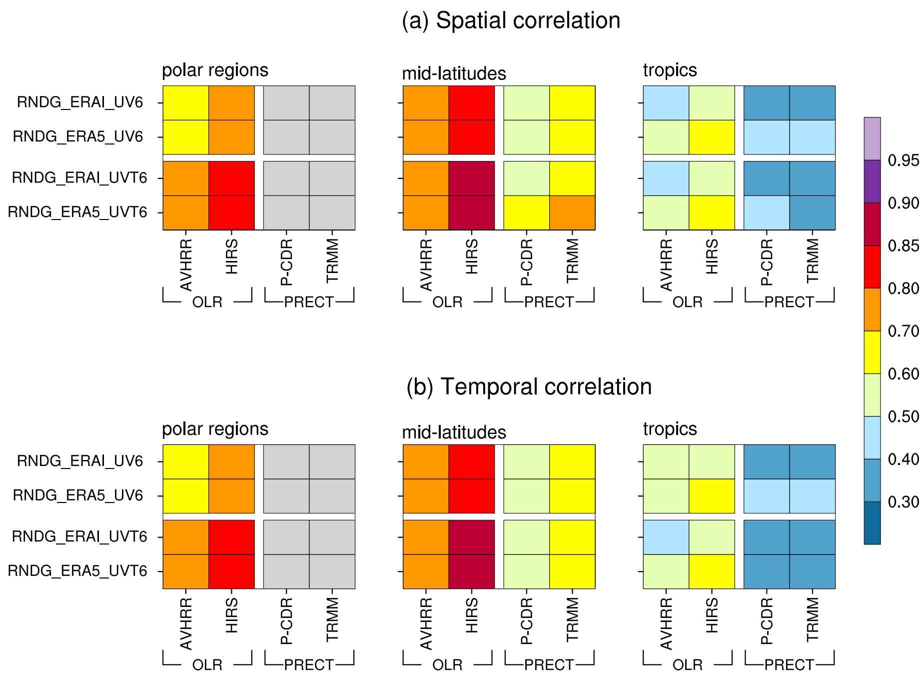

Figure 7. Anomaly correlation between simulated and observed OLR and precipitation: (a) annual mean spatial correlation; (b) spatially averaged temporal correlation. Different rows within a panel correspond to different nudged simulations. Different latitude bands are examined separately: ~~polar regions~~ the Polar Regions $(60-90°S, 60-90°N)$, the midlatitudes $(30-60°S, 30-60°N)$, and the tropics $(20°S-20°N)$. The physical quantities and sources of observational data are indicated ~~below~~ along the ~~heat maps~~x-axis in each panel. All correlations were calculated from anomalies with respect to monthly averages. Gray boxes indicate missing values resulting from observational data being unavailable. The simulation setups are described in Section 2.3 and Table 1.

Administration's (NOAA's) daily retrievals from the High Resolution Infrared Radiation Sounder ~~(Lee et al., 2007, HIRS)~~ (HIRS, Lee et al., 2007) and the Advanced Very High Resolution Radiometer ~~(AVHRR; Stowe et al., 2002)~~(AVHRR, Stowe et al., 2002) . The simulated total precipitation rate is compared with 3-hourly data from the Tropical Rainfall Measuring Mission (TRMM) 3B42V7 product (Huffman et al., 2007; Huffman and Bolvin, 2013) and daily data from the Precipitation Estimation from Remotely Sensed Information using Artificial Neural Networks-Climate Data Record (labeled as "P-CDR" in figures here, Ashouri et al., 2015). Further details of the datasets and the comparison procedure can be found in Sun et al. (2019).

The anomaly correlations shown in Fig. 7 indicate that the correlations in the high- and mid-latitude regions are very similar between the ERA5 and ERA-Interim nudged simulations regardless of whether temperature is constrained. In the low latitudes (20 °S to 20 °N), the correlations are higher when ERA5 is used as the constraining data, in terms of both OLR and precipitation, and both with or without temperature nudging. Figure 8 indicates that the changes associated with higher data frequency are small for the annual or regional averages shown here.

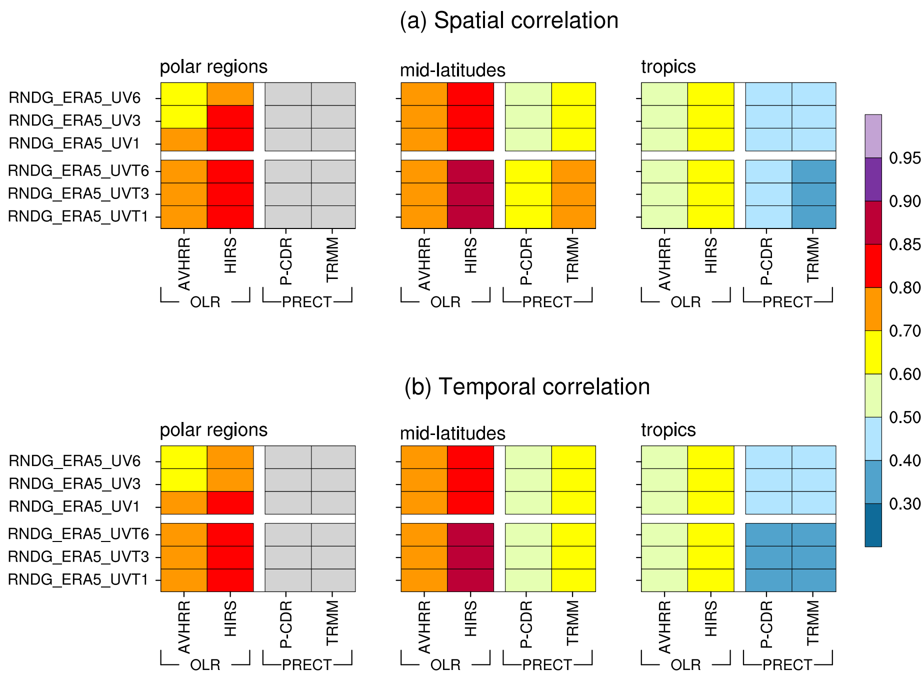

Figure 8. Similar to Fig. 7 but for simulations using different data frequencies (6-hourly, 3-hourly, or hourly). All simulations shown in this figure were nudged to the ERA5 reanalysis. Simulations shown in the top three rows of (a) and (b) used the wind-only (U, V) nudging, while simulations shown in the bottom three rows of (a) and (b) used the wind and temperature (U, V, and T) nudging.

Figure 9 evaluates the simulated zonal and temporal propagation of meridionally averaged precipitation rate in boreal spring (March to May) of 2010 over the tropical Pacific Ocean (10^{o}S–10^{o}N, 60^{o}E–90^{o}W, upper row) and North America (25^{o}N–50^{o}N, 150^{o}E-60^{o}W, lower row). Panels (a) and (d) are Hovmöller diagrams plotted from the TRMM data. The bar charts show the correlation between the Hovmöller diagram of TRMM data and the corresponding Hovmöller diagrams plotted from various nudged simulations. Consistent with the anomaly correlations shown in Figs. 7 and 8, in the tropics we see a clear improvement in the simulated propagation of precipitation when ERA5 is used as the constraining data (Fig. 9b) while in the mid-latitudes there are no substantial differences between ERA-Interim-nudged and ERA5-nudged results (Fig. 9e). The impact of frequency of the constraining data is negligible (Fig. 9c, f). ~~Same~~ The same conclusions can be drawn if we use the root-mean-squre error (RMSE) as the evaluation ~~metrics (c. f.~~ metric (cf. Figure A4), and if we change the evaluation to a different season (~~c. f.Figure~~cf. Fig. S2).

As an aside, we note that the better precipitation hindcast skills in the mid-latitudes than in the tropics (Fig. 9c versus d) are consistent with the findings in Sun et al. (2019). The impact of constraining temperature ~~appear~~ appears to be negligible for the 2010 results shown here (Fig. 9c-d, solid fill versus hatching), while Sun et al. (2019) showed better precipitation hindcast skill with additional temperature nudging for spring 2011, especially in the tropics (see Figures 6 and 7 therein). This suggests that the role of temperature nudging can be ~~case dependent~~case-dependent. Future evaluation in this aspect will be useful.

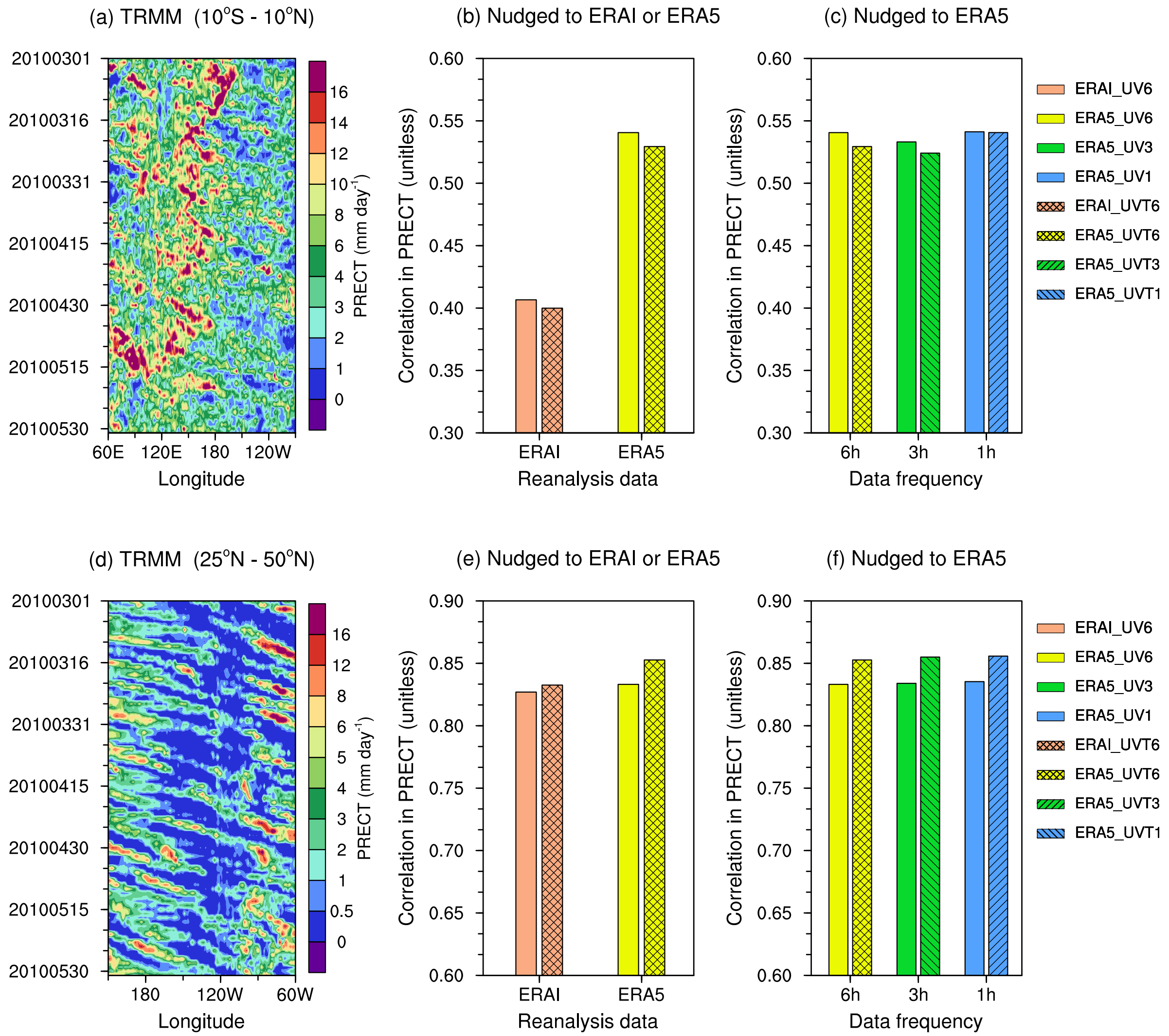

Figure 9. Evaluation of the spatio-temporal distribution of daily precipitation from 1 March to 31 May 2010 over the tropical Pacific Ocean (10^{o}S–10^{o}N, 60^{o}E–90^{o}W, upper row) and North America (25^{o}N–50^{o}N, 150^{o}E-60^{o}W, lower row). (a) and (d): Hovmöller diagram of the meridionally averaged total precipitation rates (PRECT, unit: mm day^{-1}) from TRMM. The dates are labeled along the y axis. (b–c) and (e–f): correlations between a Hovmöller diagram derived from TRMM and the Hovmöller diagram derived from various nudged simulations. Panels (b) and (e) compare simulations using ERA-Interim or ERA5 as constraining data and with or without temperature nudging. Panels (c) and (f) compare simulations with U, V or U, V, and T nudged towards ERA5 but using 6-hourly, 3-hourly, and hourly reanalysis for the constraining data. All nudged simulations shown here used the sequence of ~~calculation~~ calculations in Fig. 1b, so the prefix “RNDG_” is dropped to keep the legends short. The simulation setups are described in Section 2.3 and Table 1.

4.3 Comparison with the ARM observations

To further assess the hindcast skill of the nudged simulations, we use the radiosonde observations collected by the US Department of Energy's Atmospheric Radiation Measurement (ARM) user facility. Radiosonde data are often considered to be reliable high-accuracy measurements (Milrad, 2017) and therefore can provide an objective evaluation of model simulations. Data from three ARM atmospheric observatories are selected to cover different climate regimes, including the Southern Great Plains (SGP) site over the mid-latitude land (https://www.arm.gov/capabilities/observatories/sgp), the North Slope of Alaska (NSA) site in the NH Northern Hemisphere polar region (https://www.arm.gov/capabilities/observatories/nsa), and the Tropical Western Pacific site sites at Manus (TWPC1), Nauru (TWPC2), and Darwin (TWPC3) in the tropics (https://www.arm.gov/capabilities/observatories/twp). To our knowledge, radiosonde measurements from these sites were not used in the data assimilation system producing the ERA reanalysis products, and hence can be considered to be independent data for the evaluation of the simulations nudged to ERA-Interim or ERA5.

The simulated temperature, relative humidity, and horizontal wind speeds for winds in January 2010 are evaluated against measurements collected in the same time period at SGP (Fig. 10a-d), NSA (Fig. 10e-h), and three TWP sites (TWPC1 in Fig. 11a-d, TWPC2 in Fig. 11e-h, and TWPC3 in Fig. 11i-l)from the same time period. The ERA-Interim reanalysis (black dashed lines in the figures) and ERA5 (black solid lines) are also included for comparison. The 6-hourly model output and reanalysis products were horizontally remapped to the location of ARM site locations of ARM sites using bilinear interpolation. For each of the meteorological quantities shown here, the root-mean-square error (RMSE) between errors (RMSEs) between the ERA-nudged simulations (or ERA analyses) and the ARM measurements were calculated with all available vertical profiles at each site the sites in January 2010. The number of vertical profiles for each field For each of the variables shown in Figs. 10 and 11 (i.e., T, RH, U, or V), the numbers of available vertical profiles at SGP, NSA, TWPC1, TWPC2 and TWPC3 is were 121, 63, 49, 57 and 127, respectively (ARM observatories provide data four times a day at SGP and TWPC3, and twice a day at the NSA, TWPC1 and TWPC2). The temporal correlations between EAM simulations or ERA analyses and the ARM measurements are shown in Fig. A5 and Fig. A6 in the Appendix.

As expected, reanalyses (black lines in Fig. 10, Fig. 11, Fig. A5 and Fig. A6) show better agreement with the ARM radiosonde data compared to the nudged EAM simulations (colored lines). ERA5 (solid black in Fig. 10 and Fig. A5) is in general better than ERA-Interim (dashed black) at the mid-latitude SGP site and the high-latitude NSA site. For the three ARM TWP sites in the tropics, ERA5 is not necessarily always better than ERA-Interim. For example, ERA5's zonal wind field (U, solid black in Fig. 10d) shows larger RMSEs below 500 hPa compared to the ERA-Interim (dashed black).

The ERA-nudged simulations show good agreement with the ARM radiosonde measurements at the mid-latitude (SGP) and high-latitude (NSA) sites (Fig. 10). Compared to the ERA-Interim-nudged simulations (colored dashed lines), the ERA5-nudged simulations (colored solid lines) produce have slightly better hindcast skills. In addition, EAM simulations with temperature nudging (red, orange and green lines) show overall better hindcast skills, regardless of which ERA product was used as the constraining data. Slightly better hindcast skills for horizontal winds can be obtained by using the 3-hourly ERA5 data

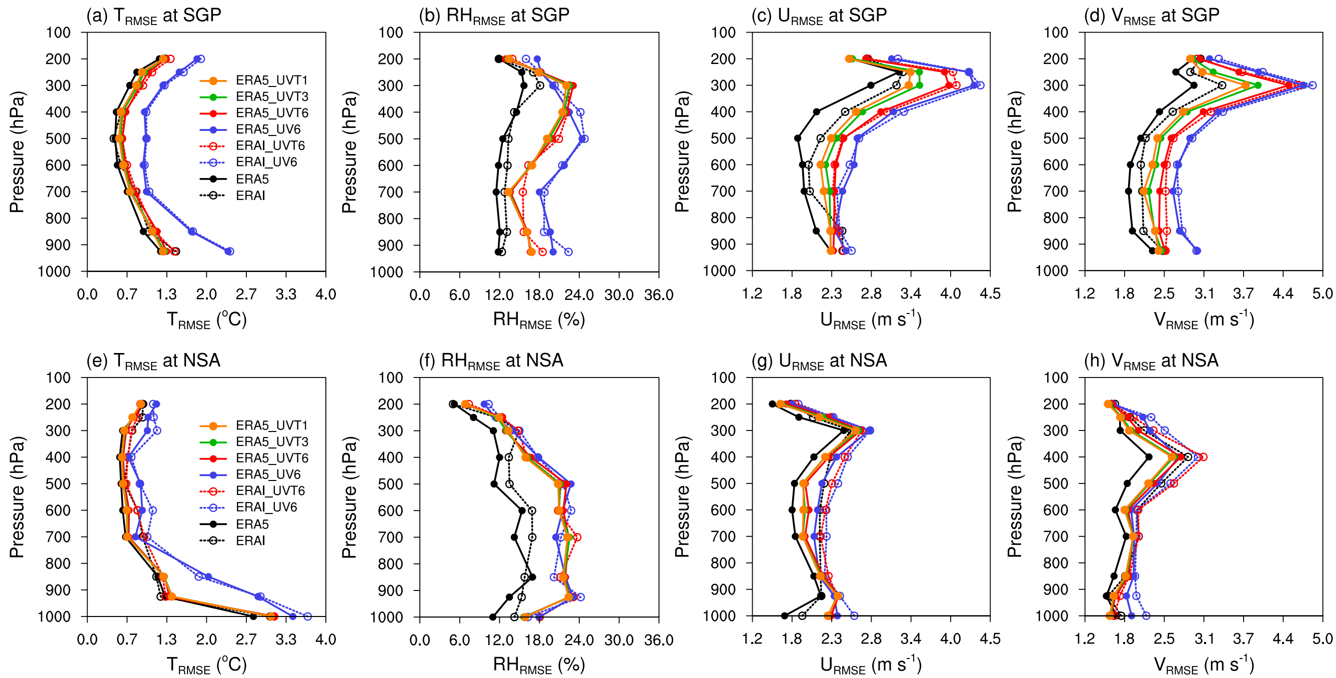

Figure 10. Comparison of two reanalysis products (ERA-Interim and ERA5, black lines) and various nudged simulations (colored lines) with ARM radiosonde measurements of January 2010 at the location of Southern Great Plains (SGP) (36.607°N, 97.488°W; panels a–d), and North Slope of Alaska (NSA) (71.323° N, 156.609° W; panels e–h), The four columns from left to right show the root-mean-square error (RMSE) in temperature (T, unit: ^{o}C), relative humidity (RH, unit: percent), zonal wind (U, unit: m s^{-1}) and meridional wind (V, unit: m s^{-1}). All nudged simulations shown here used the sequence of ~~calculation~~ calculations in Fig. 1b, so the prefix "RNDG_" is dropped in this figure to keep the labels short. The simulation setups can be found in Section 2.3 and Table 1. RMSEs were calculated from 6-hourly data for ARM SGP (121 profiles per variable) and 12-hourly data for ARM NSA (63 profiles per variable) in January 2010. ~~We note that the~~ The radiosonde ~~observation only samples twice per day~~ observations at ARM NSA site were only available twice per day. Bilinear interpolation was used to remap the reanalyses and model output to the two ARM sites.

(green lines) for nudging ~~,~~ instead of using ~~the~~ 6-hourly data (red lines). Using 3-hourly (green lines) or hourly (orange lines) constraining data gives very similar results.

Consistent with the experiences reported in the literature (e.g., Jeuken et al., 1996; Sun et al., 2019), weather events in the tropics are less well constrained by nudging. Compared to the ARM SGP and NSA sites (Fig. 10, Fig. A5), the magnitude of the RMSEs in ERA-nudged simulation at three ARM TWP sites are in ~~a similar range~~ similar ranges (Fig. 11), while the temporal correlations are smaller at the tropical sites, especially for temperature and relative humidity (Fig. A6). ~~In addition, the differences of RMSEs and temporal correlations in ERA-nudged simulations with ERA5 reanalysis and higher constraining data frequency are not obvious at the three ARM TWP sites, except that EAM simulations with~~ At the tropical sites, we do not see systematic improvements when switching from EAM-Interim to EAM5 for the constraining data or when increasing the data frequency, although the UVT nudging (red, orange and green lines in Fig. 11 and Fig. A6) still ~~show consistent~~ provides better hindcast skills than the UV nudging (blue lines).

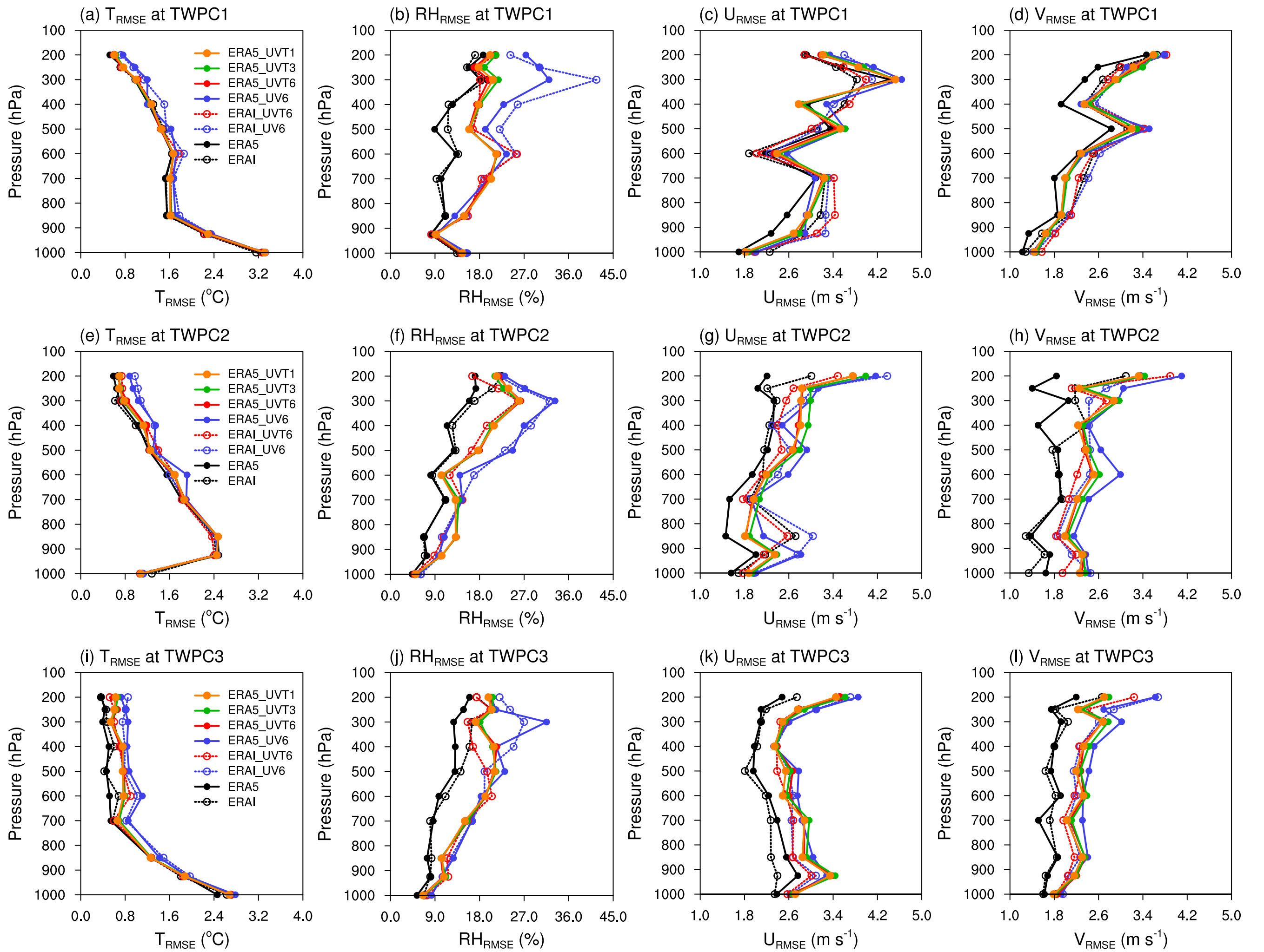

Figure 11. As in Fig. 10 but showing the root-mean-square-errors (RMSEs) at the location of Tropical Western Pacific (TWP) site at Manus (2.060° S, 147.425° E; panels a–d), Nauru (0.502° S, 166.917° E; panels e–h), and Darwin (12.425° S, 130.892° E); panels i–l). The simulation setups can be found in Section 2.3 and Table 1. RMSEs were calculated from 12-hourly data for ARM TWP1 (49 profiles per variable) and TWPC2 (57 profiles per variable), and 6-hourly data for TWPC3 (127 profiles per variable) in January 2010. We note that the radiosonde observation only samples twice per day at ARM TWPC1 and TWPC2, and four time per day at TWPC3. Bilinear interpolation was used to remap the reanalyses and model output to the three ARM sites.

5 Impact on the estimation of anthropogenic aerosol effect

Nudging has been recognized as a useful and computationally efficient technique ~~for estimating~~ to estimate the anthropogenic aerosol effect (F_{aer}) in global climate models (Kooperman et al., 2012; Zhang et al., 2014, 2016; Ghan et al., 2016; Liu et al., 2018). In this section, we evaluate the impact of nudging implementation on the estimated ~~anthropogenic aerosol effect in EAM, as it~~ F_{aer} in EAMv1. It is of practical value to identify nudging implementations capable of providing F_{aer} estimates that are consistent with those in the free-running simulations, as F_{aer} has been identified as one of the key aspects that need more attention in the future development and evaluation of EAM (Golaz et al., 2019; Zhang et al., 2022). ~~As mentioned in Section 2.3, a subset of the nudging configurations listed in Table 1 are used to conduct simulations with both the present-day (PD ,~~ Similar to previous studies, we derive F_{aer} by contrasting a pair of nudged EAMv1 simulations conducted with PD (year 2010) and ~~pre-industrial (PI ,~~ PI (year 1850) emissions of the anthropogenic aerosols and ~~their precursors to estimate F_{aer}~~ precursors following the CMIP6 protocol (Eyring et al., 2016; Hoesly et al., 2018; Feng et al., 2020).

~~Normalized global (a-b) and topical (c-d) mean annually averaged anthropogenic aerosol effect (PD-PI differences, denoted by Δ) in the free-running and nudged EAM simulations. FSNT/FLNT is the TOA net shortwave/longwave radiation flux and SWCF/LWCF the shortwave/longwave cloud radiative effects. The vertical thin line and whiskers associated to dark grey bar indicates the standard deviation of the 5-ensembles in CLIM. Results from nudged simulations are normalized by the corresponding ensemble average PD-PI differences from CLIM. The unnormalized data can be found in Table S3. The simulations are described in Section 2.3 and Table 1.~~

~~Figure **??**a–b shows the globally averaged annual mean~~ As explained in Sect. 2.3 and summarized in group 1 of Table 1, we carried out 5 pairs of 1-year simulations without nudging (the “CLIM" runs) or with very weak nudging (simulations “CLIMp1"–“CLIMp4"). The 5-member mean, one-year mean, globally averaged PD-PI ~~differences~~ difference in the top-of-atmosphere (TOA) ~~radiation fluxes and cloud radiative effects. Results from the nudged simulations are normalized by the corresponding values derived from CLIM (ensemble mean). The unnormalized data can be found in Table S3. The estimated F_{aer} (~~net radiative flux, ΔFNET~~in Table S3) in the free-running simulation~~ , is about -1.7 W m^{-2} ~~(about~~ . The shortwave component is ΔFSNT = -2.4 W m^{-2} ~~for the shortwave component and~~ , and the longwave component is ΔFLNT = -0.7 W m^{-2} ~~for the longwave). This is~~ (Table S3). These numbers are consistent with the effective aerosol forcing ~~estimate in EAMv1 reported in Golaz et al. (2019). Both of the wind-only nudged simulations (RNDG_UV~~ estimates reported in Sect. 6.1 of Golaz et al. (2019). The PD-PI differences in shortwave and longwave cloud forcings ΔSWCF = -1.7 W m^{-2} and ~~NDG_ERA5_UV) provide similar F_{aer} estimates (orange and yellow bars) as in CLIM (dark grey bars) and the differences between them are smaller than the ensemble spread in CLIM simulations.~~ ΔLWCF = 0.6 W m^{-2}, respectively (Table S3).

~~When the temperature is nudged (in addition to horizontal winds), the model nudged towards CLIM (RNDG_UVT6, blue bars) provides a reasonable estimate for the longwave, but an underestimated F_{aer} estimate for the shortwave (more than 20% reduction)~~

In Fig. 12, we compare various configurations of the nudged simulations with CLIM in terms of the annual mean PD-PI differences averaged over the globe or the tropics. All results were normalized by the ensemble mean of CLIM; the thick black

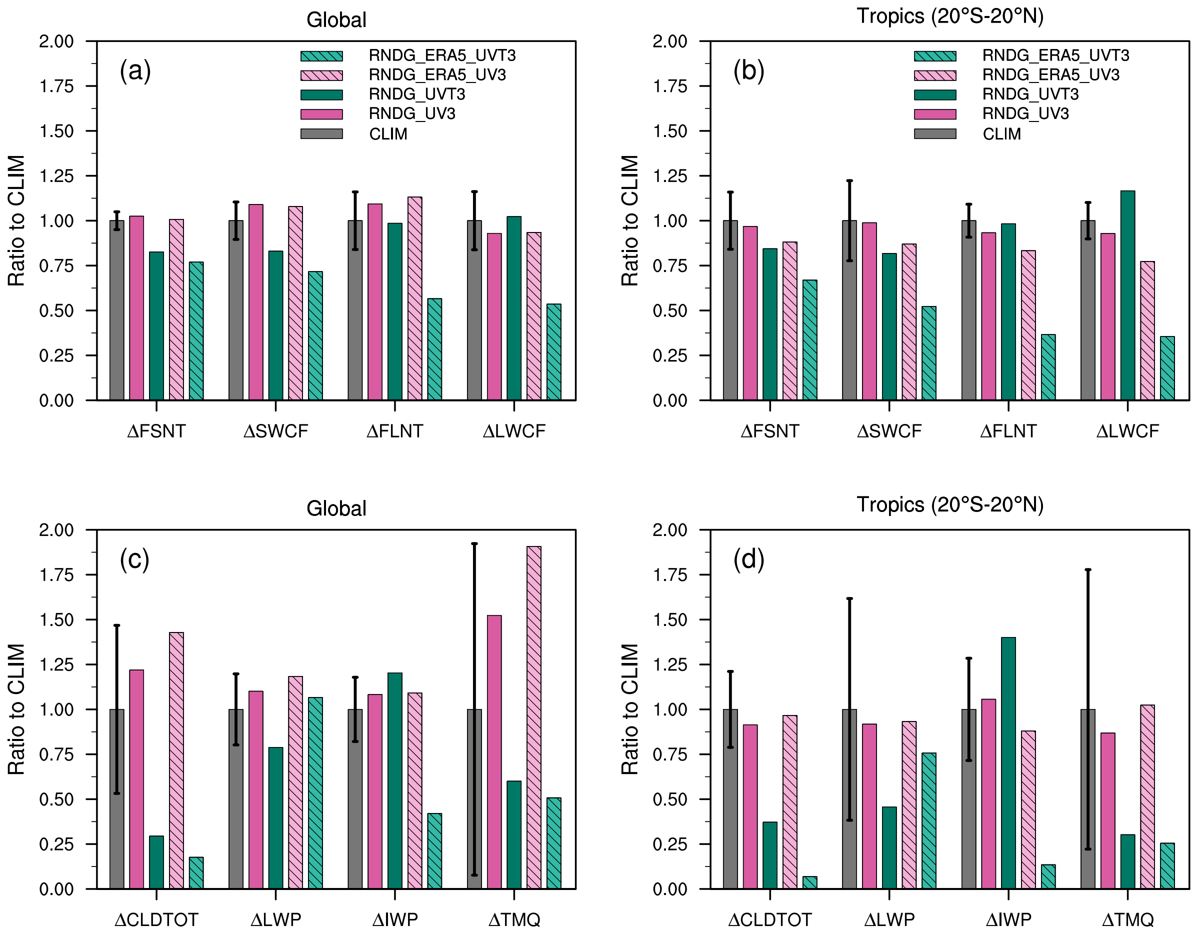

Figure 12. First row: global mean (a) and topical mean (b) annually-averaged anthropogenic aerosol effect (PD-PI differences, denoted by Δ) estimated by free-running (i.e. CLIM) and nudged EAM simulations. FSNT and FLNT are the TOA net shortwave and longwave radiation flux, respectively. SWCF and LWCF are the shortwave and longwave cloud radiative forcing, respectively. Second row: the same as in the first row but for global mean (c) and topical mean (d) annually-averaged PD-PI difference in total cloud fraction (CLDTOT), liquid water path (LWP), ice water path (IWP) and total precipitable water (TMQ). All values have been normalized by the ensemble mean of CLIM. The thick whiskers attached to the grey bars indicate the two-standard-deviation ranges of the 5-member CLIM ensemble. The non-normalized data can be found in Table S3. The simulations are described in Section 2.3 and Table 1.

whiskers attached to the gray bars indicate the two-standard-deviation ranges of the CLIM ensemble. The non-normalized data can be found in Table S3 in the supplemental materials. All of the nudged simulations shown in the figure used the revised sequence of calculations and 3-hourly constraining data. Two of the nudged simulations were constrained by ERA5 and the other two by CLIM PD. We also compare simulations conducted using UV-nudging with those using UVT-nudging. ~~The~~

Panel (a) of Fig. 12 shows the global mean PD-PI differences in the TOA fluxes and cloud forcing. Keeping in mind the ensemble spread of the CLIM simulations, we see that the estimates obtained with UV-nudging (pink bars) are consistent with the estimates from CLIM, while the estimates obtained with UVT-nudging (green bars) show statistically significant deviations from CLIM. This is true for both the ERA5-nudged and CLIM-nudged simulations, and the impact of temperature nudging is ~~much larger when EAM is nudged towards~~ considerably larger when ERA5 ~~reanalysis. Compared to the CLIM, NDG_ERA5_UVT (magenta bars) produces a more than 25% reduction for the shortwave (~~is used as the constraining data. The ΔFSNT ~~), and about a~~ estimated by NDG_ERA5_UVT3 is about 25% lower than CLIM, and the ΔFLNT is about 50% ~~reduction the longwave (~~lower than CLIM. The same qualitative conclusions can be drawn when we focus only on the tropics (panel b of Fig. 12), and the underestimation resulting from nudging temperature to ERA5 is more severe than for the global averages.

To help explain the impact of temperature nudging on the F_{aer} estimates, we show in the second row of Fig. 12 the PD-PI differences in the global and tropical mean total cloud fraction (Δ~~FLNT). The change in the~~ CLDTOT), cloud liquid and ice water path (Δ~~IWP~~ LWP and ΔIWP), and total precipitable water (ΔTMQ). All results are again normalized by the ensemble mean of CLIM, and the non-normalized data can be found in Table S3~~) also decreases by more than a factor 2. Over the tropics (Figure ??c–d and Table S4), the impact is even larger, with about 40% F_{aer} reduction in the shortwave, and about a 65% reduction in the longwave.These results are consistent with those in Zhang et al. (2014) which showed that the~~. Among the four quantities, ΔCLDTOT and ΔIWP show the largest and most significant reductions when temperature is nudged to ERA5, which can be further explained by the zonal and annual mean temperature differences (ΔT) and in-cloud ice number concentration differences (ΔICINC) shown in Fig. 13.

Fig. 13a suggests that EAMv1's climatology, when compared to ERA5, features cold biases on the order of 1-2 K in the upper troposphere over the tropical and mid-latitude regions where small ice crystals are often formed through homogeneous ice nucleation. These small ice crystals are known to have a large impact on the simulated cloud radiative forcing. Nudging EAM's temperature towards ERA5 effectively introduces bias corrections (Fig 13b) that lead to a warmer base state and weakened homogeneous ice nucleation (Fig. A7b). Consequently, the PD-PI changes in aerosol and precursor emissions cause substantially smaller ΔICNIC compared to CLIM (Fig. 13d versus c), which explains the significant reduction in ΔFLNT and ΔLWCF shown as hatched green bars in Fig. 12a–b. This reasoning is consistent with the finding in Zhang et al. (2014) that temperature nudging in ~~the CAM5 model leads to~~ EAMv1's predecessor model CAM5 led to a substantial decrease in the ice cloud amount and ~~the~~ a weaker impact of anthropogenic aerosols on longwave radiation~~is weaker. This suggests there still exist significant temperature biases in EAMv1 and the simulated ice formation is still sensitive to the anthropogenic aerosol concentrations.~~.

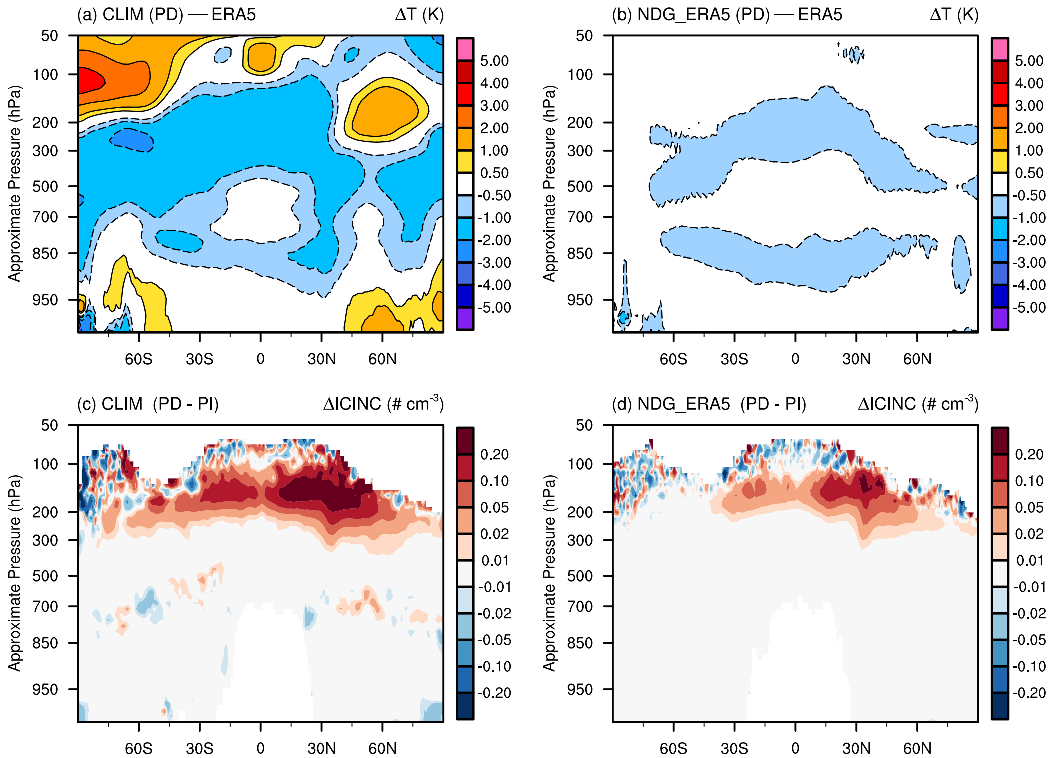

Figure 13. Upper row: zonal and annual mean differences in temperature (ΔT, unit: K) between the CLIM PD simulation and the ERA5 reanalysis (panel a), and between a nudged PD simulation and ERA5 (panel b). The nudged simulation is labeled as "NDG_ERA5 (PD)" for brevity in panel b; it correspond to the simulation RNDG_ERA5_UVT3 in Table 1 performed with PD emissions of aerosols and precursors. Lower row: PD-PI differences of in-cloud ice number concentration (ΔICINC, unit: # cm^{-3}) derived from free-running (i.e. CLIM) simulations (panel c) and from EAMv1 simulations UVT-nudging towards ERA5 (i.e. RNDG_ERA5_UVT3, panel d). Details of simulation setup can be found in Sect. 2.3 and Table 1.

Figure 12a–b indicates that when EAMv1 simulations are nudged to its own climatology, constraining temperature also has significant impacts on the estimated ΔFSNT and ΔSWCF (see green versus pink bars with solid fill). This is mainly due to the constrained temperature adjustment to the aerosol perturbation, since the PD and PI simulations were nudged towards the same CLIM PD simulation. The anthropogenic aerosols and precursors are known to have significant impacts on air temperature (Fig. A8a). When only the horizontal winds are nudged towards CLIM PD, the impacts of anthropogenic aerosols and precursors on temperature are smaller than in the free-running simulations but nevertheless still sizable (Fig. A8b). In contrast, the nudging of temperature substantially reduces the PD-PI temperature differences as expected (Fig. A8c). The results shown in Fig. A8 suggest that the constrained temperature response mainly affects the simulated PD-PI changes in cloud liquid mass (ΔCLDLIQ, Fig. A8, second row) and cloud ice mass (ΔCLDICE, Fig. A8, third row) in the middle and lower troposphere (i.e., below 500hPa). This explains why the solid green bars in Fig. 12 deviate from the gray bars more in the shortwave radiation than in the longwave component.

Overall, consistent with previous studies using other global aerosol-climate models (e.g. Kooperman et al., 2012; Zhang et al., 2014; Gha , our results indicate that nudging the horizontal winds but not temperature towards the ERA5 reanalysis or EAM's own meteorology is the preferred simulation configuration to estimate F_{aer}. When only the winds are nudged, we expect changing the nudging tendency calculation location or using high-frequency nudging data won't have a significant impact on The temperature nudging needs to be applied with caution, as the potential climatology discrepancies between CLIM and reanalysis might lead to large biases in the F_{aer} estimation.

In Figure 14, we evaluate the impact of the frequency of the constraining data. At least for the global and annual mean F_{aer}, the results obtained from simulations using 6-hourly constraining data (orange bars in the figure) are very similar to those obtained using 3-hourly constraining data (blue bars), regardless of whether UV-nudging (Fig. 14, upper row) or UVT-nudging (Fig. 14, lower row) is used. The small impact of constraining data frequency on global and tropical mean F_{aer} , since the impact on estimates is expected. As shown in Section 3.2, the impact of constraining data frequency on present-day simulations are already very small. is sizable only in limited regions where strong diurnal variations exist. Therefore, using 6-hourly constraining data in nudged simulations is sufficient for estimating the time-mean F_{aer}.

6 Conclusions

Nudging has been widely used in the development and evaluation of global and regional atmospheric models. In this work, we further improved the nudging implementation in EAMv1 (Sun et al., 2019) compared to the work of Sun et al. (2019) and evaluated the impact on the climate representation, nudged hindcast skill representativeness, the hindcast skill of nudged simulations, and the estimation of anthropogenic aerosol effect in the model. effects.

The study was motivated by an unresolved issue in Sun et al. (2019), namely a nudged EAMv1 simulation constrained by EAMv1's own meteorology showed non-negligible local deviations from the baseline, with annually averaged SWCF changes on the order of annually-averaged SWCF changes as large as 4–8 W m^{-2} over some of the subtropical marine stratocumulus and trade cumulus regions. Two reasons were identified: First, EAMv1 outputs meteorological fields (from a baseline simulation) for nudging before the radiation parameterization, but the nudging tendency is calculated at a different place (location in the time integration loop, i.e., after the dynamical core). This inconsistency introduced an extra term in unintended contribution to the nudging tendency that was proportional to the effect of deep convection, shallow convection, and cloud microphysics on the simulated atmosphere (Section 3.1). Second, the EAM-simulated winds and temperature in the lower troposphere were found to have high-frequency modes with non-negligible magnitudes. For example, the zonal wind in the Peruvian stratocumulus region was found to have a prominent 12-hour cycle. Such variations cannot be properly captured by a 6-hourly sampling frequency, hence resulting in significant aliasing issues with the constraining data used for nudging (Section 3.2). We showed that by moving the calculation of nudging tendency to the same location as data output (Fig. 1b) and by increasing the frequency of constraining data to 3-hourly, one could largely remove the discrepancies between a 1° free-running EAMv1 sim-

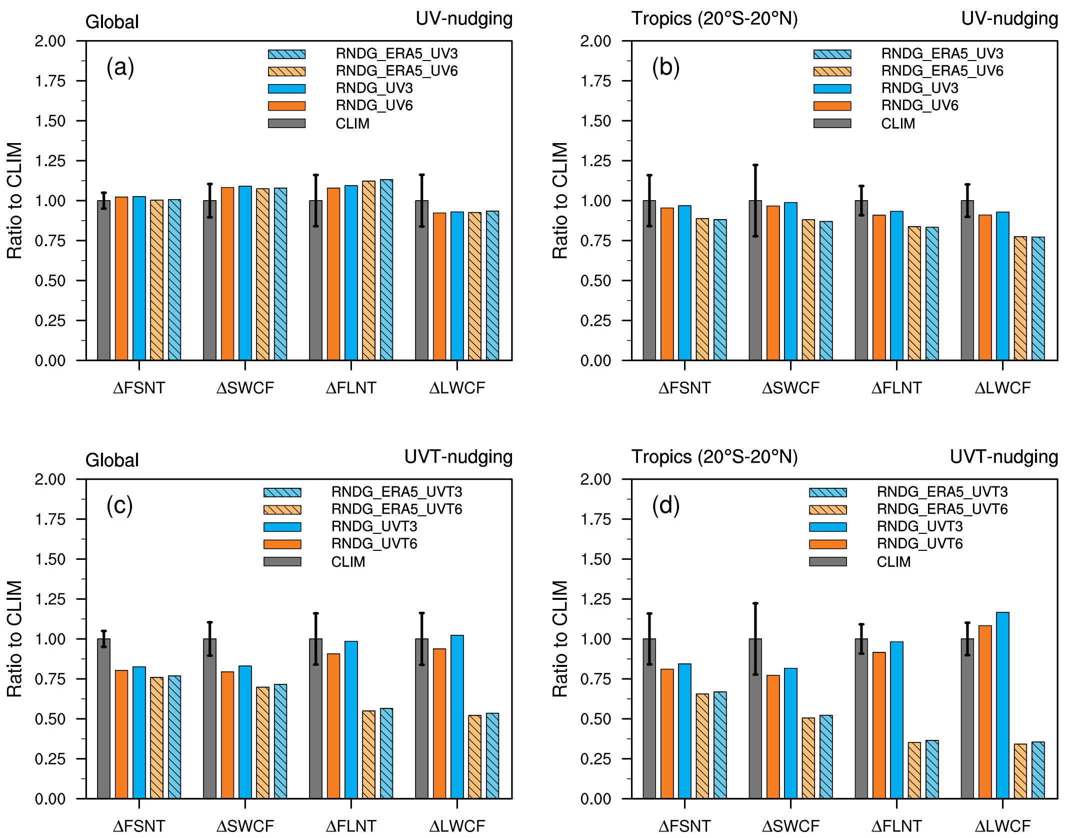

Figure 14. Global mean (a, c) and topical mean (b, d) annually-averaged anthropogenic aerosol effect (PD-PI differences, denoted by Δ) estimated by free-running (i.e. CLIM, grey bars) and nudged EAM simulations (colored bars). FSNT and FLNT are the TOA net shortwave and longwave radiation flux, respectively. SWCF and LWCF are the shortwave and longwave cloud radiative forcing, respectively. All values have been normalized by the ensemble mean of CLIM. The thick whiskers attached to the grey bars indicate the two-standard-deviation ranges of the 5-member CLIM ensemble. The upper row compares the UV-nudged simulations with CLIM, and the lower row compares the UVT-nudged simulations with CLIM. The solid color bars indicate simulations nudged towards CLIM; the hatched color bars indicate simulations nudged towards ERA5 reanalysis. Orange and blue bars correspond to nudged simulations performed with 6-hourly and 3-hourly constraining data, respectively. The simulations are described in Section 2.3 and Table 1.

ulation and a 1° nudged simulation constrained by EAM's own meteorology. Further increasing the data frequency to hourly only provided marginal improvements. For future studies that nudge EAM towards its own meteorology, we recommend using the revised implementation and the 3-hourly constraining data ~~.~~ for 1° simulations. Whether higher horizontal resolution can benefit from higher data frequency remains to be investigated. In Table A1~~shows an example on how to use the revised nudging implementation~~ , we have provided the nudging-related *namelist* settings for two of the simulations discussed in this paper to demonstrate how to turn on the revised sequence of calculations and change the constraining data frequency~~via *namelist* changes~~.

~~These~~ The abovementioned improvements further motivated us to investigate the potential benefits of using the ERA5 reanalysis data, which are available at a higher frequency compared to ERA-Interim, for nudged hindcast simulations. In terms of the annual mean fields, there were discernible but small regional changes when switching from ERA-Interim to ERA5 or changing the constraining data frequency ~~with~~ when using ERA5. The impacts on global mean climate were found to be small (Section 4.1). Satellite retrievals ~~for~~ of OLR and precipitation were used to evaluate the model~~hindcast~~ 's skill in capturing real weather events. When ERA5 was used instead of ERA-Interim, the simulated OLR and precipitation ~~are~~ were significantly improved, especially in the tropics. We also evaluated the ~~model~~ nudged simulations using radiosonde measurements from ~~three ARM sites that have very different climate conditions. The simulated meteorological fields (~~several ARM sites in different climate regimes. At the SGP and NSA sites, the simulated horizontal winds, temperature, and relative humidity ~~) were~~ were systematically improved when replacing ERA-Interim with ERA5 and when using higher-frequency nudging data~~are used~~. Significant improvements are seen in the mid and high-latitude ARM sites~~(SGP and NSA), but there are no tangible improvements at~~ . At the tropical sites (~~TWPC1-3)~~TWPC1, TWPC2, and TWPC3), the improvements were not as significant. At SGP and NSA, nudging winds and temperature together ~~can~~ was found to further improve the ~~model hindcast skill . The overall good agreements in the meteorological conditions between the nudged EAMv1 simulations and ARM observations provide~~ hindcast skill of the simulations. Overall, the good agreement in the simulated and observed meteorological conditions provides a good basis for ~~using~~ possible future studies that use ARM measurements to ~~identify parameterizations~~ help identify parameterization deficiencies and improve the representation of cloud and ~~aerosol related atmospheric processes~~ aerosol-related atmospheric processes in EAM.

Last but not least, we evaluated the impact of nudging ~~implementation~~ on the estimated anthropogenic aerosol ~~indirect~~ effects (F_{aer}). Results show that ~~when only winds in EAMv1 are nudged either towards a baseline simulation or ERA5 reanalysis, the estimated global~~ the frequency of the constraining data has negligible impacts on the estimated global and tropical averages of annual mean F_{aer}~~is very close to the estimates from free-running simulations. Consistent with Zhang et al. (2014), EAMv1 simulations nudged to temperature from the ERA5 reanalysis show significant changes in the~~ . Similar to conclusions from earlier studies, we recommend nudging the horizontal winds but not the air temperature when attempting to obtain estimates of F_{aer} ~~estimates when compared with the~~ that are consistent with the estimates from free-running ~~baseline. In particular, the longwave F_{aer} estimated from the EAMv1 simulations nudged towards ERA5 reanalysis is a factor of 2 smaller compared to the free-running baseline. Therefore, for the~~ simulations. The reason is twofold: when nudging toward a reanalysis product, the effective temperature bias correction introduced by nudging can significantly change the model's mean climate and consequently change the simulated clouds and the estimates of F_{aer}estimate, nudging the horizontal winds but not temperature is still the preferred simulation configuration for EAM; when nudging toward the model's own meteorology, nudging temperature in addition to horizontal winds can result in a strongly constrained temperature response to the aerosol perturbation, and subsequently change the simulated F_{aer}.

We note that the 1-degree configuration of EAM 1° configuration of EAMv1 was used in this study. The benefits of higher the temporal and spatial resolutions of the ERA5 data might not have be fully revealedyetbeen fully revealed. As pointed out by Jeuken et al. (1996), the linear temporal interpolation in nudging can become more questionable for higher-resolution simulations as more small short time scale processes are resolved. Also, compared to ERA-Interim, the high-resolution ERA5 data can provide more accurate meteorological variables at model resolved scalefiner spatial scales, so the ERA5-nudged simulation might perform even better at high resolutions than seen in the 1° simulations discussed here. The high-resolution configuration of EAMv1 is substantially more expensive, so and hence was not used in this studywe were not able to evaluate the nudging application at higher resolutions. However, with the upcoming release of EAMv2, the use of the new physics grid (Hannah et al., 2021) and semi-Largragian semi-Lagrangian advection scheme (Bradley et al., 2019) can will substantially reduce the costcomputational cost. It will be useful to further explore nudged EAM simulations at higher resolutions. Further work is needed to investigate whether there is additional benefit of using ERA5 in the global high-resolution simulations .

Appendix A: Supporting Information

A1 Nudging-related namelist setups for EAMv1 simulations

Table A1. List of the setups for nudging-related namelist variables in DNDG_ERAI_UVT6 and RNDG_ERA5_UVT3 conducted with EAMv1 in this study. The nudging-related setups in DNDG_ERAI_UVT6 followed the default EAMv1 with the sequence of ~~calculation~~ calculations shown in Fig 1a. The RNDG_ERAI_UVT6 used the sequence of ~~calculation~~ calculations shown in Fig 1b with the revised nudging-related setups (rows in bold face) suggested by this study. See Table 1 and Section 2.3 in the main text for the detailed descriptions for DNDG_ERAI_UVT6 and RNDG_ERA5_UVT3.

&nudging_nl	DNDG_ERAI_UVT6	RNDG_ERA5_UVT3
nudge_model	.True.	.True.
nudge_method	'Linear'	'Linear'
nudge_currentstep	.False.	.False.
Nudge_loc_physout	**.False.**	**.True.**
nudge_tau	6.0	6.0
model_times_per_day	48	48
nudge_times_per_day	**4**	**8**
nudge_ucoef	1.0	1.0
nudge_uprof	1	1
nudge_vcoef	1.0	1.0
nudge_vprof	1	1
nudge_tcoef	1.0	1.0
nudge_tprof	1	1
nudge_qcoef	0.0	0.0
nudge_qprof	0	0
nudge_pscoef	0.0	0.0
nudge_psprof	0	0
nudge_path	'./ERA-Interim/'	'./ERA5/'
nudge_file_template	'interim_se_%y-%m-%d-%s.nc'	'era5_ne30L72_%y-%m-%d-%s.nc'
nudge_file_ntime	1	1
nudge_beg_year	2009	2009
nudge_beg_month	10	10
nudge_beg_day	1	1
nudge_end_year	2011	2011
nudge_end_month	1	1
nudge_end_day	1	1

A2 Method to generate error metrics for Figure 5

The physical qualities listed in Table A2 are used to construct the error metics for the evaluation of nudged simulations in EAMv1. These physical quantities have also been widely used to evaluate climate model fidelity (e.g., Donahue and Caldwell, 2018; Wan et al., 2021). The error metrics as shown in Figure 5 include the relative differences in the simulated global averages and the relative differences in global patterns between the test simulations and the reference simulation conducted by EAM. Following Wan et al. (2021), the relative difference in simulated global averages are defined as the mean differences between the test simulation and reference simulation, normalized by the annual mean value from the reference simulation. While the relative difference in global pattern is defined as the centered root-mean-square (RMS) differences of the patterns between the test simulation and reference simulation, normalized by the RMS of the pattern in the reference simulation. A “pattern" here represents the annal mean, global, geographical distribution of a physical quantity.

Table A2. List of observational data and EAM's output used for evaluating the nudged simulations. The observational data were obtained from NCAR AMWG diagnostics package (http://www.cgd.ucar.edu/amp/amwg/diagnostics/plotType.html).

Physical quantity	EAM output
Surface longwave downwelling flux	FLDS
Surface net longwave flux	FLNS
TOA upward longwave flux	FLUT
TOA clearsky upward longwave flux	FLUTC
Surface net shortwave flux	FSNS
TOA net shortwave flux	FSNTOA
TOA clearsky net shortwave flux	FSNTOAC
Longwave cloud forcing	LWCF
Shortwave cloud forcing	SWCF
Total cloud amount	CLDTOT
200 hPa zonal wind	U
500 hPa geopotential height	Z3
Precipitation rate	PRECT
Total precipitable water	TMQ
Sea level pressure	PSL
Surface latent heat flux	LHFLX
Surface sensible heat flux	SHFLX
Surface stress	TAUX, TAUY
2m air temperature	TREFHT
Sea level temperature on land	TS

A3 Additional figures

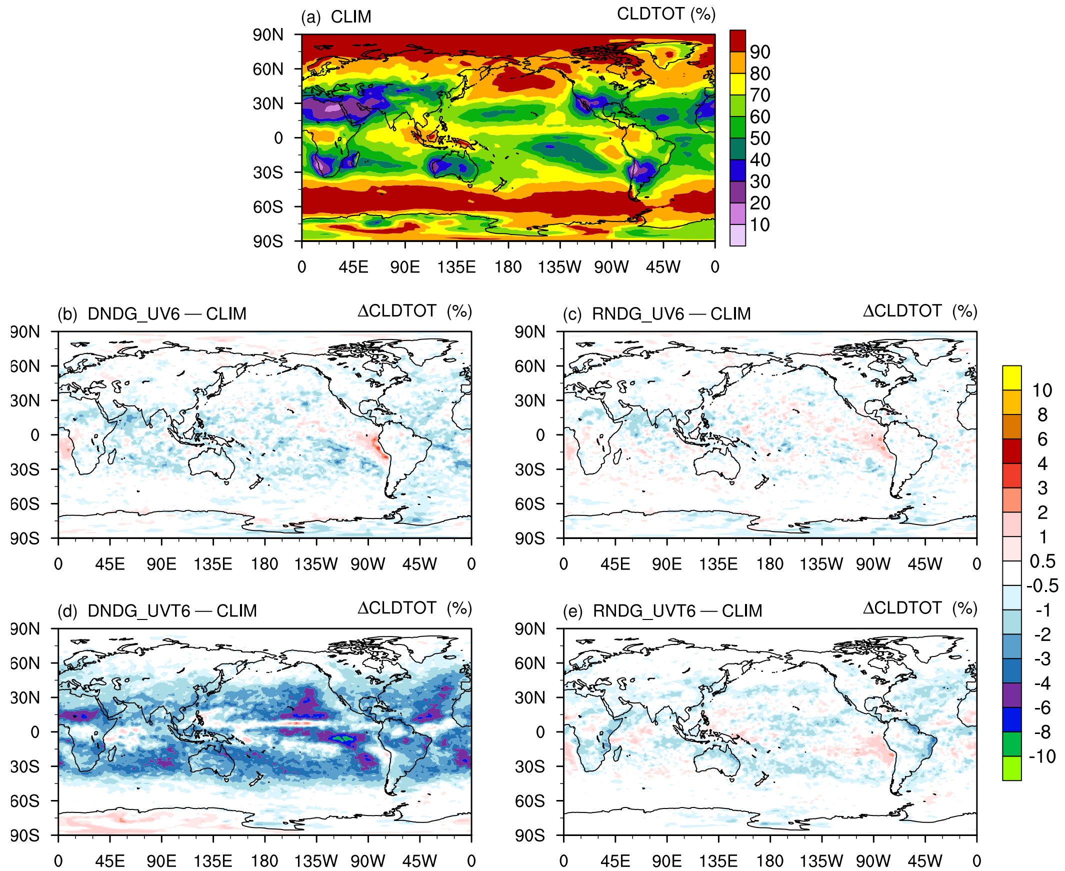

Figure A1. As in Figure 2 but showing results for the total cloud fraction fields (CLDTOT, unit: percent). The simulation setups are described in Section 2.3 and Table 1.

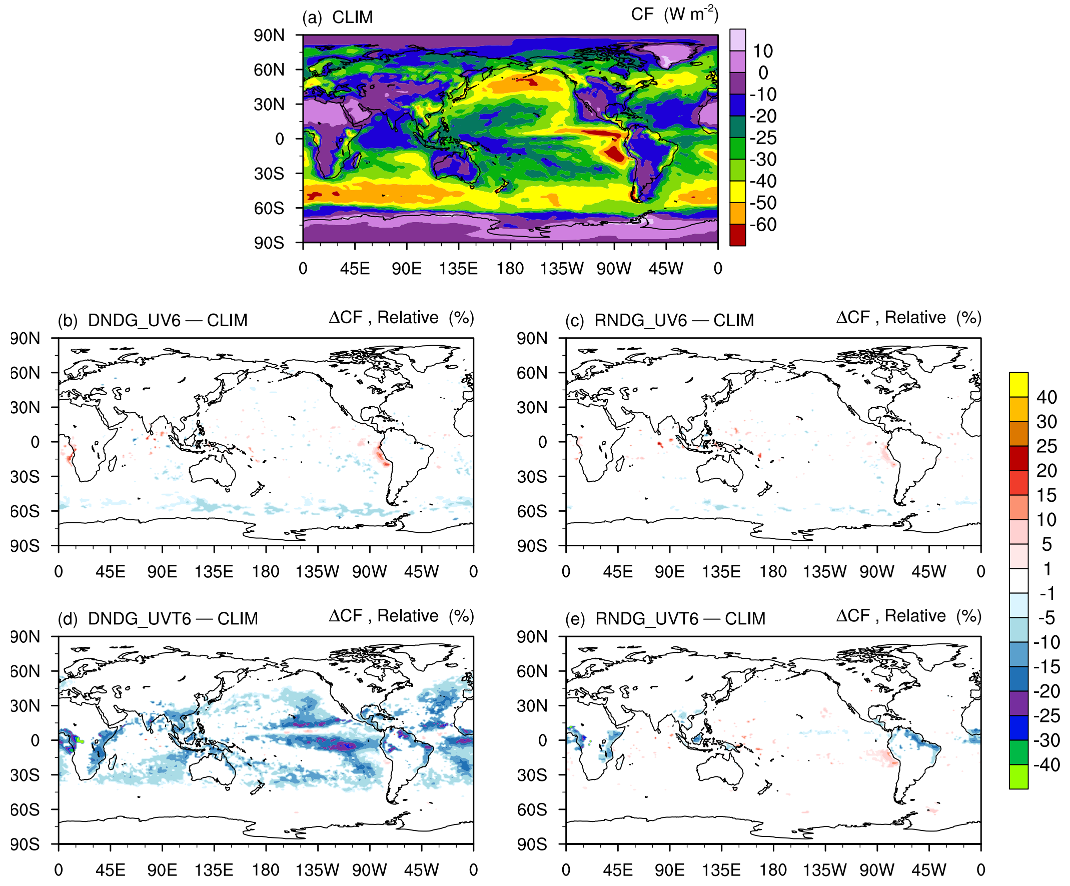

Figure A2. As in Fig. 2 but showing the relative differences in total cloud forcing (CF, unit: W m^{-2}) in panels (b)–(e). The simulation setups are described in Section 2.3 and Table 1.

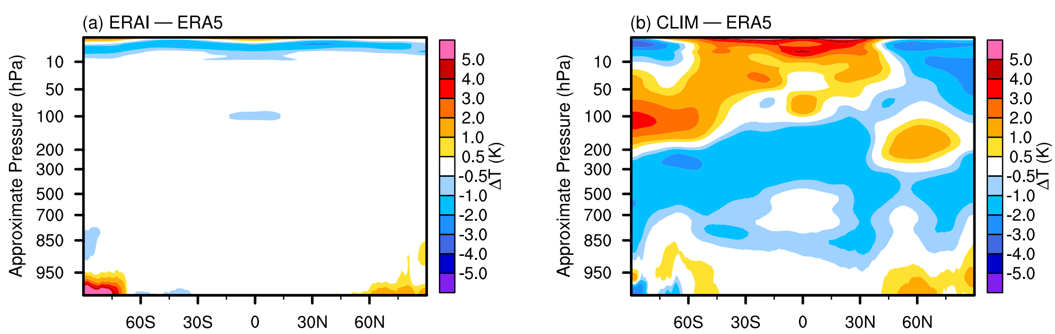

Figure A3. Year 2010 annual mean zonally averaged temperature differences (Δ T, unit: K) between ERA-Interim ("ERAI") and ERA5 (panel a), and between EAMv1's free-running simulation CLIM and ERA5 (panel b).

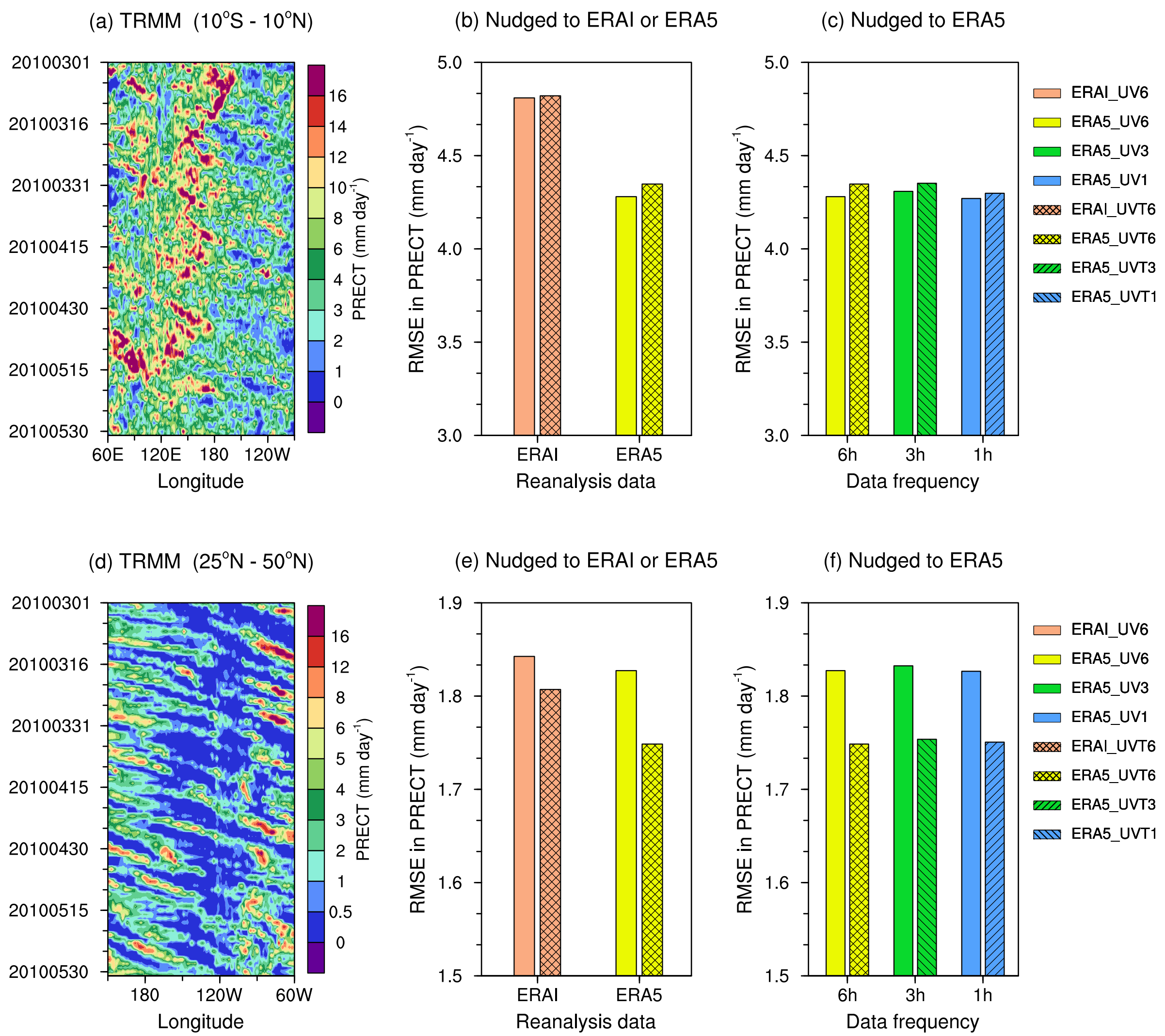

Figure A4. As in Figure 9 but the root-mean-square-errors (RMSEs) between a Hovmöller diagram derived from TRMM and the Hovmöller diagram derived from various nudged simulations are shown in panels (b–c) and (e–f). The simulation setups are described in Section 2.3 and Table 1.

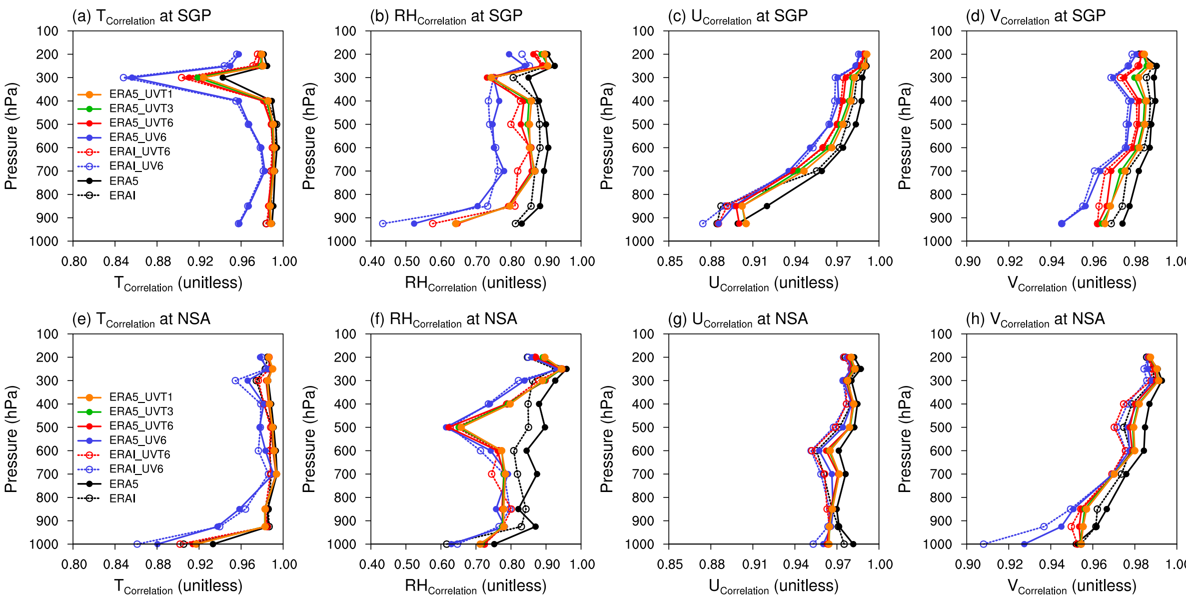

Figure A5. As in Fig. 10 but showing the temporal correlations between various nudged simulations (colored lines) or reanalysis products (ERA-Interim and ERA5, black lines) and the ARM measurements. The simulation setups are described in Section 2.3 and Table 1.

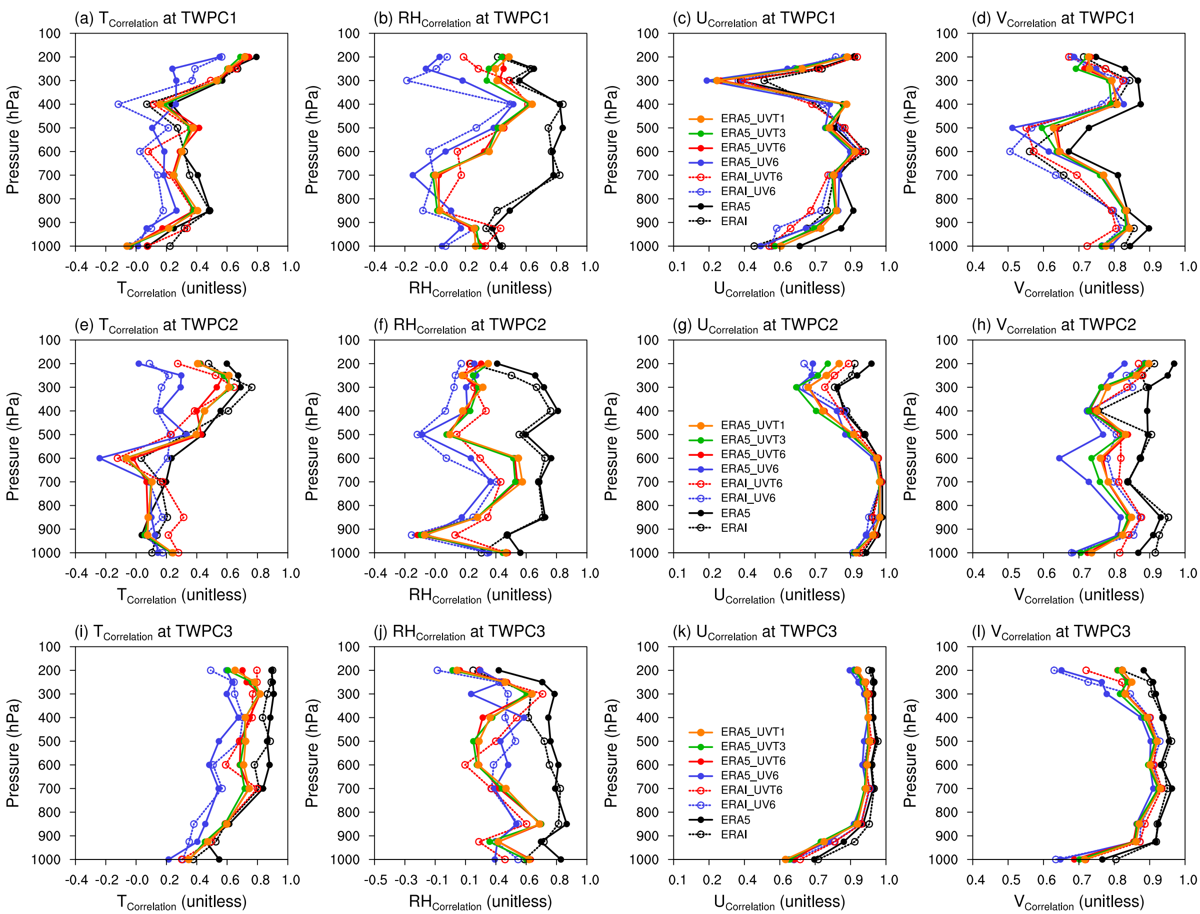

Figure A6. As in Fig. 11 but showing the temporal correlations between various nudged simulations (colored lines) or reanalysis products (ERA-Interim and ERA5, black lines) and the ARM measurements. The simulation setups are described in Section 2.3 and Table 1.

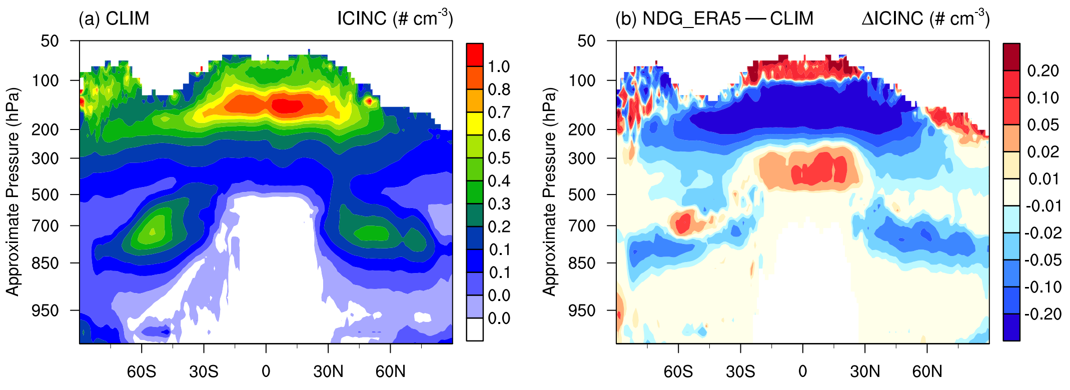

Figure A7. Annual mean zonally averaged (a) in-cloud ice number concentration (ICINC, unit: # cm^{-3}) from EAMv1 free-running simulation (i.e., CLIM), and (b) difference in ICINC (ΔICINC, unit: # cm^{-3}) between CLIM and nudged EAMv1 simulation. The NDG_ERA5 in the figure caption is the acronym of RNDG_ERA5_UVT3 (nudged towards 3-hourly wind and temperature fields from ERA5 reanalysis). All simulations used present-day (PD) aerosol emissions. See details in Section 2.3 and Table 1.

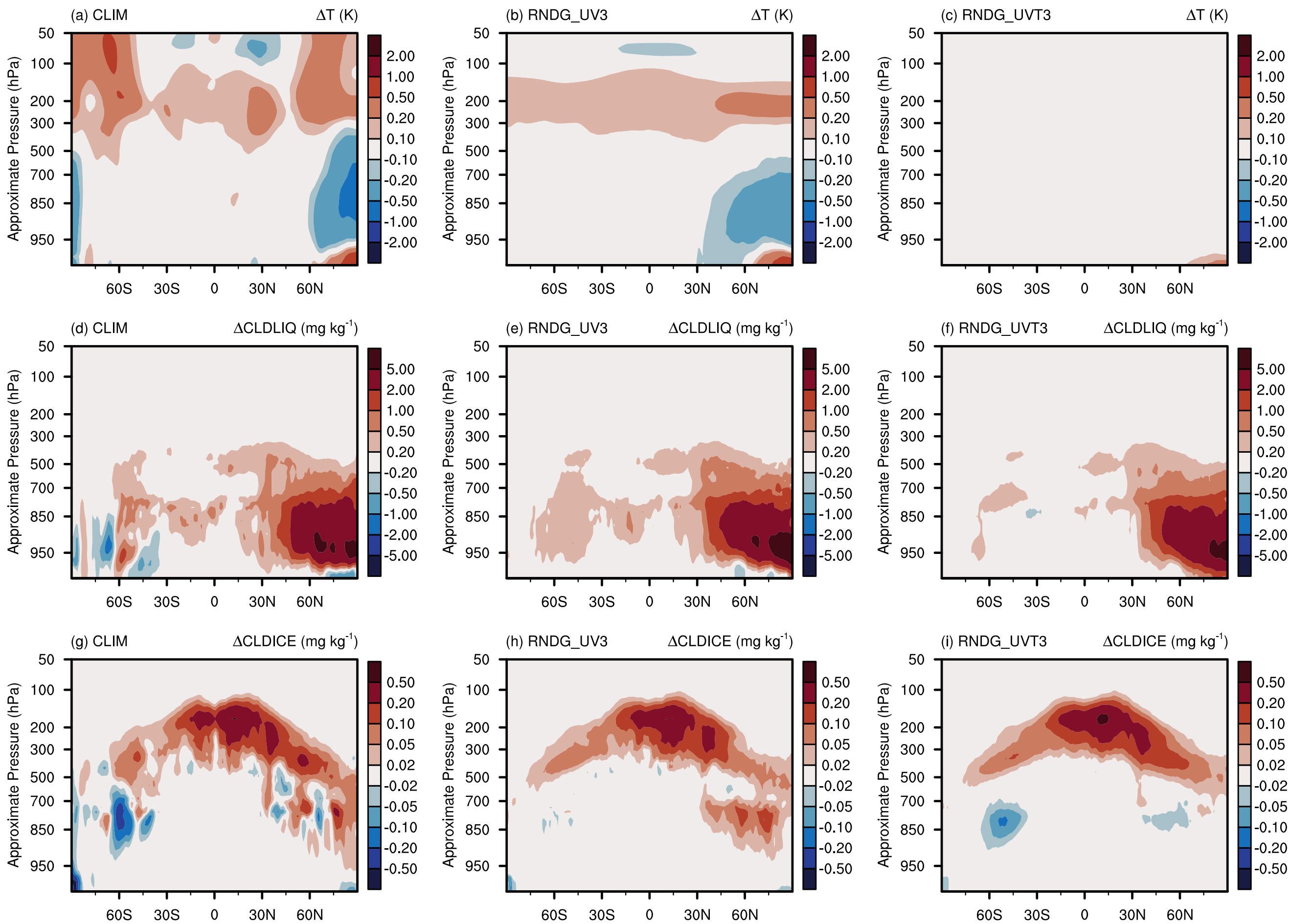

Figure A8. PD-PI differences in temperature (ΔT, unit: K, top row), cloud liquid water mixing ratio (ΔCLDLIQ, unit: mg kg^{-1}, middle row) and cloud ice water mixing ratio (ΔCLDICE, unit: mg kg^{-1}, bottom row) from the free-running (i.e. CLIM) and nudged EAM simulations. RNDG_UVT3 (second column) is for wind-only nudging, and RNDG_UVT3 (third column) is for nudging to both wind and temperature fields. The 3-hourly constraining data frequency is used for all nudged simulations. Both PD and PI simulations are nudged to CLIM (PD meteorology) in EAMv1. See details in Section 2.3 and Table 1.

Code availability. The EAMv1 source code and run scripts used in this study can be found on Zenodo at https://doi.org/10.5281/zenodo.5532606 (E3SM developers et al., 2021).

Data availability. The data for the analyses in this study can be found on Zenodo at https://doi.org/10.5281/zenodo.6728357 (Zhang and Zhang, 2022). Radiosonde measurements at the SGP, NSA, TWPC1, TWPC2 and TWPC3 sites were obtained from the ARM user facility (http://dx.doi.org/10.5439/1021460), a DOE Office of Science user facility managed by BER. Satellite data used in this paper were obtained from the following sources

– https://pmm.nasa.gov/data-access/downloads/trmm for the TRMM 3B42 precipitation data,

– https://climatedataguide.ucar.edu/climate-data/persiann-cdr-precipitation-estimation-remotely-sensed-information-using-artificial for the PERSIANN-CDR precipitation data,

– https://climatedataguide.ucar.edu/climate-data/outgoing-longwave-radiation-olr-hirs for the HIRS OLR data,

– https://www.esrl.noaa.gov/psd/data/gridded/data.interp_OLR.html for the AVHRR OLR data.

Author contributions. KZ and HW initiated this study. HW identified the two nudging implementation issues. SZ conducted all simulations, processed the model output, and carried out the analyses with input from KZ and HW. SZ, KZ, and HW wrote the paper. All co-authors contributed to the revision.

Competing interests. The authors declare no competing interests

Acknowledgements. We thank the two anonymous reviewers for their helpful comments and suggestions. SZ and KZ were supported by the Laboratory Directed Research and Development Program at Pacific Northwest National Laboratory (PNNL), a multiprogram national laboratory operated by Battelle for the U.S. Department of Energy (DOE) under contract DE-AC05-76RL01830. KZ was also supported by DOE Office of Science, Office of Biological and Environmental Research (BER) via the Energy Exascale Earth System Model (E3SM) project. HW was supported by DOE~~BER via the~~ 's Scientific Discovery through Advanced Computing (SciDAC) program ~~(grant number: 70276).~~ through a partnership in Earth system model development between BER and the Advanced Scientific Computing Research (ASCR), grant number 70276. The EAMv1 code (DOI:10.11578/E3SM/dc.20180418.36) was obtained from the E3SM project sponsored by DOE BER. Computing resources were provided by DOE BER Earth System Modeling program's Compy computing cluster located at PNNL.

References

Ashouri, H., Hsu, K.-L., Sorooshian, S., Braithwaite, D. K., Knapp, K. R., Cecil, L. D., Nelson, B. R., and Prat, O. P.: PERSIANN-CDR: Daily precipitation climate data record from multisatellite observations for hydrological and climate studies, Bulletin of the American Meteorological Society, 96, 69–83, 2015.

Bradley, A. M., Bosler, P. A., Guba, O., Taylor, M. A., and Barnett, G. A.: Communication-Efficient Property Preservation in Tracer Transport, SIAM Journal on Scientific Computing, 41, C161–C193, https://doi.org/10.1137/18M1165414, 2019.

Dee, D. P., Uppala, S. M., Simmons, A. J., Berrisford, P., Poli, P., Kobayashi, S., Andrae, U., Balmaseda, M. A., Balsamo, G., Bauer, P., Bechtold, P., Beljaars, A. C. M., van de Berg, L., Bidlot, J., Bormann, N., Delsol, C., Dragani, R., Fuentes, M., Geer, A. J., Haimberger, L., Healy, S. B., Hersbach, H., Hólm, E. V., Isaksen, L., Kållberg, P., Köhler, M., Matricardi, M., McNally, A. P., Monge-Sanz, B. M., Morcrette, J.-J., Park, B.-K., Peubey, C., de Rosnay, P., Tavolato, C., Thépaut, J.-N., and Vitart, F.: The ERA-Interim reanalysis: configuration and performance of the data assimilation system, Quarterly Journal of the Royal Meteorological Society, 137, 553–597, https://doi.org/10.1002/qj.828, 2011.

Dennis, J. M., Edwards, J., Evans, K. J., Guba, O., Lauritzen, P. H., Mirin, A. A., St-Cyr, A., Taylor, M. A., and Worley, P. H.: CAM-SE: A scalable spectral element dynamical core for the Community Atmosphere Model,, Int. J. High Perform., 26, 74–89, https://doi.org/10.1177/1094342011428142, 2012.

Donahue, A. S. and Caldwell, P. M.: Impact of physics parameterization ordering in a global atmosphere model, Journal of Advances in Modeling Earth Systems, 10, 481–499, https://doi.org/10.1002/2017MS001067, 2018.

E3SM developers, Zhang, S., Zhang, K., and Sun, J.: EAM source code and scripts for nudging experiments in Zhang et. al. (2022, GMDD), https://doi.org/10.5281/zenodo.5532606, 2021.

Eyring, V., Bony, S., Meehl, G. A., Senior, C. A., Stevens, B., Stouffer, R. J., and Taylor, K. E.: Overview of the Coupled Model Intercomparison Project Phase 6 (CMIP6) experimental design and organization, Geoscientific Model Development, 9, 1937–1958, https://doi.org/10.5194/gmd-9-1937-2016, 2016.

Fast, J. D., Berg, L. K., Zhang, K., Easter, R. C., Ferrare, R. A., Hair, J. W., Hostetler, C. A., Liu, Y., Ortega, I., Sedlacek III, A., Shilling, J. E., Shrivastava, M., Springston, S. R., Tomlinson, J. M., Volkamer, R., Wilson, J., Zaveri, R. A., and Zelenyuk, A.: Model representations of aerosol layers transported from North America over the Atlantic Ocean during the Two-Column Aerosol Project, Journal of Geophysical Research: Atmospheres, 121, 9814–9848, https://doi.org/https://doi.org/10.1002/2016JD025248, 2016.

Feng, L., Smith, S. J., Braun, C., Crippa, M., Gidden, M. J., Hoesly, R., Klimont, Z., van Marle, M., van den Berg, M., and van der Werf, G. R.: The generation of gridded emissions data for CMIP6, Geoscientific Model Development, 13, 461–482, https://doi.org/10.5194/gmd-13-461-2020, 2020.

Gates, W. L., Boyle, J. S., Covey, C., Dease, C. G., Doutriaux, C. M., Drach, R. S., Fiorino, M., Gleckler, P. J., Hnilo, J. J., Marlais, S. M., Phillips, T. J., Potter, G. L., Santer, B. D., Sperber, K. R., Taylor, K. E., and Williams, D. N.: An Overview of the Results of the Atmospheric Model Intercomparison Project (AMIP I), Bulletin of the American Meteorological Society, 80, 29–56, https://doi.org/10.1175/1520-0477(1999)080<0029:AOOTRO>2.0.CO;2, 1999.

Gelaro, R., McCarty, W., Suárez, M. J., Todling, R., Molod, A., Takacs, L., Randles, C. A., Darmenov, A., Bosilovich, M. G., Reichle, R., Wargan, K., Coy, L., Cullather, R., Draper, C., Akella, S., Buchard, V., Conaty, A., da Silva, A. M., Gu, W., Kim, G.-K., Koster, R., Lucchesi, R., Merkova, D., Nielsen, J. E., Partyka, G., Pawson, S., Putman, W., Rienecker, M., Schubert, S. D., Sienkiewicz, M., and

Zhao, B.: The Modern-Era Retrospective Analysis for Research and Applications, Version 2 (MERRA-2), Journal of Climate, 30, 5419 – 5454, https://doi.org/10.1175/JCLI-D-16-0758.1, 2017.

Gettelman, A. and Morrison, H.: Advanced two-moment bulk microphysics for global models, Part I: Off-line tests and comparison with other schemes, Journal of Climate, 28, 1268–1287, https://doi.org/10.1175/JCLI-D-14-00102.1, 2015.

Ghan, S., Wang, M., Zhang, S., Ferrachat, S., Gettelman, A., Griesfeller, J., Kipling, Z., Lohmann, U., Morrison, H., Neubauer, D., Partridge, D. G., Stier, P., Takemura, T., Wang, H., and Zhang, K.: Challenges in constraining anthropogenic aerosol effects on cloud radiative forcing using present-day spatiotemporal variability, Proceedings of the National Academy of Sciences, 113, 5804–5811, https://doi.org/10.1073/pnas.1514036113, 2016.

Golaz, J.-C., Larson, V., and Cotton, W.: A PDF-Based Model for Boundary Layer Clouds. Part I: Method and Model Description, Journal of the Atmospheric Sciences, 59, 3540–3551, https://doi.org/10.1175/1520-0469(2002)059<3540:APBMFB>2.0.CO;2, 2002.

Golaz, J.-C., Caldwell, P. M., Van Roekel, L. P., Petersen, M. R., Tang, Q., Wolfe, J. D., Abeshu, G., Anantharaj, V., Asay-Davis, X. S., Bader, D. C., Baldwin, S. A., Bisht, G., Bogenschutz, P. A., Branstetter, M., Brunke, M. A., Brus, S. R., Burrows, S. M., Cameron-Smith, P. J., Donahue, A. S., Deakin, M., Easter, R. C., Evans, K. J., Feng, Y., Flanner, M., Foucar, J. G., Fyke, J. G., Griffin, B. M., Hannay, C., Harrop, B. E., Hoffman, M. J., Hunke, E. C., Jacob, R. L., Jacobsen, D. W., Jeffery, N., Jones, P. W., Keen, N. D., Klein, S. A., Larson, V. E., Leung, L. R., Li, H.-Y., Lin, W., Lipscomb, W. H., Ma, P.-L., Mahajan, S., Maltrud, M. E., Mametjanov, A., McClean, J. L., McCoy, R. B., Neale, R. B., Price, S. F., Qian, Y., Rasch, P. J., Reeves Eyre, J. E. J., Riley, W. J., Ringler, T. D., Roberts, A. F., Roesler, E. L., Salinger, A. G., Shaheen, Z., Shi, X., Singh, B., Tang, J., Taylor, M. A., Thornton, P. E., Turner, A. K., Veneziani, M., Wan, H., Wang, H., Wang, S., Williams, D. N., Wolfram, P. J., Worley, P. H., Xie, S., Yang, Y., Yoon, J.-H., Zelinka, M. D., Zender, C. S., Zeng, X., Zhang, C., Zhang, K., Zhang, Y., Zheng, X., Zhou, T., and Zhu, Q.: The DOE E3SM Coupled Model Version 1: Overview and Evaluation at Standard Resolution, Journal of Advances in Modeling Earth Systems, 11, 2089–2129, https://doi.org/https://doi.org/10.1029/2018MS001603, 2019.

Hannah, W. M., Bradley, A. M., Guba, O., Tang, Q., Golaz, J.-C., and Wolfe, J.: Separating Physics and Dynamics Grids for Improved Computational Efficiency in Spectral Element Earth System Models, Journal of Advances in Modeling Earth Systems, 13, e2020MS002 419, https://doi.org/https://doi.org/10.1029/2020MS002419, 2021.

Hersbach, H., Bell, B., Berrisford, P., Hirahara, S., Horányi, A., Muñz Sabater, J., Nicolas, J., Peubey, C., Radu, R., Schepers, D., Simmons, A., Soci, C., Abdalla, S., Abellan, X., Balsamo, G., Bechtold, P., Biavati, G., Bidlot, J., Bonavita, M., De Chiara, G., Dahlgren, P., Dee, D., Diamantakis, M., Dragani, R., Flemming, J., Forbes, R., Fuentes, M., Geer, A., Haimberger, L., Healy, S., Hogan, R. J., Hólm, E., Janisková, M., Keeley, S., Laloyaux, P., Lopez, P., Lupu, C., Radnoti, G., de Rosnay, P., Rozum, I., Vamborg, F., Villaume, S., and Thépaut, J.-N.: The ERA5 global reanalysis, Quarterly Journal of the Royal Meteorological Society, 146, 1999–2049, https://doi.org/https://doi.org/10.1002/qj.3803, 2020.

Hoesly, R. M., Smith, S. J., Feng, L., Klimont, Z., Janssens-Maenhout, G., Pitkanen, T., Seibert, J. J., Vu, L., Andres, R. J., Bolt, R. M., Bond, T. C., Dawidowski, L., Kholod, N., Kurokawa, J.-I., Li, M., Liu, L., Lu, Z., Moura, M. C. P., O'Rourke, P. R., and Zhang, Q.: Historical (1750–2014) anthropogenic emissions of reactive gases and aerosols from the Community Emissions Data System (CEDS), Geoscientific Model Development, 11, 369–408, https://doi.org/10.5194/gmd-11-369-2018, 2018.

Huffman, G. J. and Bolvin, D. T.: TRMM and other data precipitation data set documentation, NASA, Greenbelt, USA, 28, 1, 2013.

Huffman, G. J., Bolvin, D. T., Nelkin, E. J., Wolff, D. B., Adler, R. F., Gu, G., Hong, Y., Bowman, K. P., and Stocker, E. F.: The TRMM multisatellite precipitation analysis (TMPA): Quasi-global, multiyear, combined-sensor precipitation estimates at fine scales, Journal of hydrometeorology, 8, 38–55, 2007.

Iacono, M. J., Delamere, J. S., Mlawer, E. J., Shephard, M. W., Clough, S. A., and Collins, W. D.: Radiative forcing by long–lived greenhouse gases: Calculations with the AER radiative transfer models, Journal of Geophysical Research: Atmospheres, 113, D13 103, https://doi.org/10.1029/2008JD009944, 2008.

Jeuken, A. B. M., Siegmund, P. C., Heijboer, L. C., Feichter, J., and Bengtsson, L.: On the potential of assimilating meteorological analyses in a global climate model for the purpose of model validation, Journal of Geophysical Research: Atmospheres, 101, 16 939–16 950, https://doi.org/10.1029/96JD01218, 1996.

Kanamitsu, M., Ebisuzaki, W., Woollen, J., Yang, S.-K., Hnilo, J. J., Fiorino, M., and Potter, G. L.: NCEP–DOE AMIP-II Reanalysis (R-2), Bulletin of the American Meteorological Society, 83, 1631 – 1644, https://doi.org/10.1175/BAMS-83-11-1631, 2002.

Kooperman, G. J., Pritchard, M. S., Ghan, S. J., Wang, M., Somerville, R. C. J., and Russell, L. M.: Constraining the influence of natural variability to improve estimates of global aerosol indirect effects in a nudged version of the Community Atmosphere Model 5, Journal of Geophysical Research: Atmospheres, 117, https://doi.org/10.1029/2012JD018588, 2012.

Larson, V. E., Golaz, J.-C., and Cotton, W. R.: A PDF-Based Model for Boundary Layer Clouds. Part I: Method and Model Description, Journal of the Atmospheric Sciences, 59, 3519–3539, https://doi.org/10.1175/1520-0469(2002)059<3519:SSAMVI>2.0.CO;2, 2002.

Lee, H.-T., Gruber, A., Ellingson, R. G., and Laszlo, I.: Development of the HIRS Outgoing Longwave Radiation Climate Dataset, Journal of Atmospheric and Oceanic Technology, 24, 2029 – 2047, https://doi.org/10.1175/2007JTECHA989.1, 2007.

Lin, G., Wan, H., Zhang, K., Qian, Y., and Ghan, S. J.: Can nudging be used to quantify model sensitivities in precipitation and cloud forcing?, Journal of Advances in Modeling Earth Systems, 8, 1073–1091, https://doi.org/10.1002/2016MS000659, 2016.

Liu, X., Ma, P.-L., Wang, H., Tilmes, S., Singh, B., Easter, R. C., Ghan, S. J., and Rasch, P.: Description and evaluation of a new four–mode version of the Modal Aerosol Module (MAM4) within version 5.3 of the Community Atmosphere Model, Geoscientific Model Development, 9, 505–522, https://doi.org/doi.org/10.5194/gmd-9-505-2016, 2016.

Liu, Y., Zhang, K., Qian, Y., Wang, Y., Zou, Y., Song, Y., Wan, H., Liu, X., and Yang, X.-Q.: Investigation of short-term effective radiative forcing of fire aerosols over North America using nudged hindcast ensembles, Atmospheric Chemistry and Physics, 18, 31–47, https://doi.org/10.5194/acp-18-31-2018, 2018.

Lohmann, U. and Hoose, C.: Sensitivity studies of different aerosol indirect effects in mixed-phase clouds, Atmospheric Chemistry and Physics, 9, 8917–8934, https://doi.org/10.5194/acp-9-8917-2009, 2009.

Ma, H.-Y., Chuang, C. C., Klein, S. A., Lo, M.-H., Zhang, Y., Xie, S., Zheng, X., Ma, P.-L., Zhang, Y., and Phillips, T. J.: An improved hindcast approach for evaluation and diagnosis of physical processes in global climate models, Journal of Advances in Modeling Earth Systems, 7, 1810–1827, https://doi.org/10.1002/2015MS000490, 2015.

Ma, P.-L., Rasch, P. J., Fast, J. D., Easter, R. C., Gustafson Jr., W. I., Liu, X., Ghan, S. J., and Singh, B.: Assessing the CAM5 physics suite in the WRF-Chem model: implementation, resolution sensitivity, and a first evaluation for a regional case study, Geoscientific Model Development, 7, 755–778, https://doi.org/10.5194/gmd-7-755-2014, 2014.

Milrad, S.: Synoptic analysis and forecasting: An introductory toolkit, Elsevier, https://doi.org/https://doi.org/10.1016/C2015-0-05604-0, 2017.

Mlawer, E. J., Taubman, S. J., Brown, P. D., Iacono, M. J., and Clough, S. A.: Radiative transfer for inhomogeneous atmospheres: RRTM, a validated correlated?k model for the longwave, Journal of Geophysical Research: Atmospheres, 102, 16,663–16,682, https://doi.org/10.1029/97JD00237, 1997.

Morrison, H. and Gettelman, A.: A New Two-Moment Bulk Stratiform Cloud Microphysics Scheme in the Community Atmosphere Model, Version 3 (CAM3). Part I: Description and Numerical Tests, Journal of Climate, 21, 3642–3659, https://doi.org/10.1175/2008JCLI2105.1, 2008.

Oleson, K., Lawrence, D., Gordon, B. B., Drewniak, B., Huang, M., Koven, C. D., Levis, S., Li, F., Riley, W. J., Subin, Z. M., Swenson, S. C., Thornton, P. E., Bozbiyik, A., Fisher, R., Heald, C. L., Kluzek, E., Lamarque, J., Lawrence, P. J., R., L. L., Sacks, W., Sun, Y., Tang, J., and Yang, Z.: Technical description of version 4.5 of the Community Land Model (CLM), Ncar technical note ncar/tn-503+str, NCAR, https://doi.org/10.5065/D6RR1W7M, 2013.

Rasch, P. J., Xie, S., Ma, P.-L., Lin, W., Wang, H., Tang, Q., Burrows, S. M., Caldwell, P., Zhang, K., Easter, R. C., Cameron-Smith, P., Singh, B., Wan, H., Golaz, J.-C., Harrop, B. E., Roesler, E., Bacmeister, J., Larson, V. E., Evans, K. J., Qian, Y., Taylor, M., Leung, L. R., Zhang, Y., Brent, L., Branstetter, M., Hannay, C., Mahajan, S., Mametjanov, A., Neale, R., Richter, J. H., Yoon, J.-H., Zender, C. S., Bader, D., Flanner, M., Foucar, J. G., Jacob, R., Keen, N., Klein, S. A., Liu, X., Salinger, A., Shrivastava, M., and Yang, Y.: An Overview of the Atmospheric Component of the Energy Exascale Earth System Model, Journal of Advances in Modeling Earth Systems, 11, 2377–2411, https://doi.org/10.1029/2019MS001629, 2019.

Reynolds, R. W., Rayner, N. A., Smith, T. M., Stokes, D. C., and Wang, W.: An Improved In Situ and Satellite SST Analysis for Climate, Journal of Climate, 15, 1609–1625, https://doi.org/10.1175/1520-0442(2002)015<1609:AIISAS>2.0.CO;2, 2002.

Separovic, L., de Elía, R., and Laprise, R.: Impact of spectral nudging and domain size in studies of RCM response to parameter modification, Climate dynamics, 38, 1325–1343, https://doi.org/10.1007/s00382-011-1072-7, 2012.

Stowe, L. L., Jacobowitz, H., Ohring, G., Knapp, K. R., and Nalli, N. R.: The Advanced Very High Resolution Radiometer (AVHRR) Pathfinder Atmosphere (PATMOS) Climate Dataset: Initial Analyses and Evaluations, Journal of Climate, 15, 1243 – 1260, https://doi.org/10.1175/1520-0442(2002)015<1243:TAVHRR>2.0.CO;2, 2002.

Subramanian, A. C. and Zhang, G. J.: Diagnosing MJO hindcast biases in NCAR CAM3 using nudging during the DYNAMO field campaign, Journal of Geophysical Research: Atmospheres, 119, 7231–7253, https://doi.org/10.1002/2013JD021370, 2014.

Sun, J., Zhang, K., Wan, H., Ma, P.-L., Tang, Q., and Zhang, S.: Impact of Nudging Strategy on the Climate Representativeness and Hindcast Skill of Constrained EAMv1 Simulations, Journal of Advances in Modeling Earth Systems, 11, 3911–3933, https://doi.org/10.1029/2019MS001831, 2019.

Taylor, M. A., Cyr, A. S., and Fournier, A.: A Non-oscillatory Advection Operator for the Compatible Spectral Element Method,, International Conference on Computational Science, Springer, Berlin, Heidelberg, https://doi.org/10.1007/978-3-642-01973-9_31, 2010.

Telford, P. J., Braesicke, P., Morgenstern, O., and Pyle, J. A.: Technical Note: Description and assessment of a nudged version of the new dynamics Unified Model, Atmospheric Chemistry and Physics, 8, 1701–1712, https://doi.org/10.5194/acp-8-1701-2008, 2008.

Wan, H., Rasch, P. J., Zhang, K., Qian, Y., Yan, H., and Zhao, C.: Short ensembles: an efficient method for discerning climate-relevant sensitivities in atmospheric general circulation models, Geoscientific Model Development, 7, 1961–1977, https://doi.org/10.5194/gmd-7-1961-2014, 2014.

Wan, H., Zhang, S., Rasch, P. J., Larson, V. E., Zeng, X., and Yan, H.: Quantifying and attributing time step sensitivities in present-day climate simulations conducted with EAMv1, Geoscientific Model Development, 14, 1921–1948, https://doi.org/10.5194/gmd-14-1921-2021, 2021.

Wan, H., Zhang, K., Rasch, P. J., Larson, V. E., Zeng, X., Zhang, S., and Dixon, R.: CondiDiag1.0: a flexible online diagnostic tool for conditional sampling and budget analysis in the E3SM atmosphere model (EAM), Geoscientific Model Development, 15, 3205–3231, https://doi.org/10.5194/gmd-15-3205-2022, 2022.

Wang, H., Easter, R. C., Zhang, R., Ma, P.-L., Singh, B., Zhang, K., Ganguly, D., Rasch, P. J., Burrows, S. M., Ghan, S. J., Lou, S., Qian, Y., Yang, Y., Feng, Y., Flanner, M., Leung, L. R., Liu, X., Shrivastava, M., Sun, J., Tang, Q., Xie, S., and Yoon, J.-H.: Aerosols in the E3SM Version 1: New Developments and Their Impacts on Radiative Forcing, Journal of Advances in Modeling Earth Systems, 12, e2019MS001 851, https://doi.org/https://doi.org/10.1029/2019MS001851, 2020.

Wang, Y., Liu, X., Hoose, C., and Wang, B.: Different contact angledistributions for heterogeneous ice nucleation in the CommunityAtmospheric Model version 5,, Atmospheric Chemistry and Physics, 14, 10 411–10 430, https://doi.org/doi.org/10.5194/acp-14-10411-2014, 2014.

Xie, S., Lin, W., Rasch, P. J., Ma, P.-L., Neale, R., Larson, V. E., Qian, Y., Bogenschutz, P. A., Caldwell, P., Cameron-Smith, P., Golaz, J.-C., Mahajan, S., Singh, B., Tang, Q., Wang, H., Yoon, J.-H., Zhang, K., and Zhang, Y.: Understanding Cloud and Convective Characteristics in Version 1 of the E3SM Atmosphere Model, Journal of Advances in Modeling Earth Systems, 10, 2618–2644, https://doi.org/https://doi.org/10.1029/2018MS001350, 2018.

Zhang, G. J. and McFarlane, N. A.: Sensitivity of climate simulations to the parameterization of cumulus convection in the Canadian Climate Centre general circulation model, Atmos. Ocean, 33, 407–446, https://doi.org/10.1080/07055900.1995.9649539, 1995.

Zhang, K., O'Donnell, D., Kazil, J., Stier, P., Kinne, S., Lohmann, U., Ferrachat, S., Croft, B., Quaas, J., Wan, H., Rast, S., and Feichter, J.: The global aerosol-climate model ECHAM-HAM, version 2: sensitivity to improvements in process representations, Atmospheric Chemistry and Physics, 12, 8911–8949, https://doi.org/10.5194/acp-12-8911-2012, 2012.

Zhang, K., Wan, H., Liu, X., Ghan, S. J., Kooperman, G. J., Ma, P.-L., Rasch, P. J., Neubauer, D., and Lohmann, U.: Technical Note: On the use of nudging for aerosol-climate model intercomparison studies, Atmospheric Chemistry and Physics, 14, 8631–8645, https://doi.org/10.5194/acp-14-8631-2014, 2014.

Zhang, K., Rasch, P. J., Taylor, M. A., Wan, H., Leung, R., Ma, P.-L., Golaz, J.-C., Wolfe, J., Lin, W., Singh, B., Burrows, S., Yoon, J.-H., Wang, H., Qian, Y., Tang, Q., Caldwell, P., and Xie, S.: Impact of numerical choices on water conservation in the E3SM Atmosphere Model version 1 (EAMv1), Geoscientific Model Development, 11, 1971–1988, https://doi.org/10.5194/gmd-11-1971-2018, 2018.

Zhang, K., Zhang, W., Wan, H., Rasch, P. J., Ghan, S. J., Easter, R. C., Shi, X., Wang, Y., Wang, H., Ma, P.-L., Zhang, S., Sun, J., Burrows, S., Shrivastava, M., Singh, B., Qian, Y., Liu, X., Golaz, J.-C., Tang, Q., Zheng, X., Xie, S., Lin, W., Feng, Y., Wang, M., Yoon, J.-H., and Leung, R. L.: Effective radiative forcing of anthropogenic aerosols in E3SMv1: historical changes, causality, decomposition, and parameterization sensitivities, Atmospheric Chemistry and Physics Discussions, 2022, 1–49, https://doi.org/10.5194/acp-2021-1087, 2022.

Zhang, S. and Zhang, K.: Data for the analyses in Zhang et. al. (2022, GMDD), https://doi.org/10.5281/zenodo.5839008, 2022.

Zhang, S., Wang, M., Ghan, S. J., Ding, A., Wang, H., Zhang, K., Neubauer, D., Lohmann, U., Ferrachat, S., Takeamura, T., Gettelman, A., Morrison, H., Lee, Y., Shindell, D. T., Partridge, D. G., Stier, P., Kipling, Z., and Fu, C.: On the characteristics of aerosol indirect effect based on dynamic regimes in global climate models, Atmospheric Chemistry and Physics, 16, 2765–2783, https://doi.org/10.5194/acp-16-2765-2016, 2016.